

Effective Dynamics, Big Bounces and Scaling Symmetry in Bianchi Type I Loop Quantum Cosmology

Dah-Wei Chiou*

*Institute for Gravitation and the Cosmos, Physics Department,
The Pennsylvania State University, University Park, PA 16802, U.S.A.*

The detailed formulation for loop quantum cosmology (LQC) in the Bianchi I model with a scalar massless field has been constructed. In this paper, its effective dynamics is studied in two improved strategies for implementing the LQC discreteness corrections. Both schemes show that the big bang is replaced by the big bounces, which take place up to three times, once in each diagonal direction, when the area or volume scale factor approaches the critical values in the Planck regime measured by the reference of the scalar field momentum. These two strategies give different evolutions: In one scheme, the effective dynamics is independent of the choice of the finite sized cell prescribed to make Hamiltonian finite; in the other, the effective dynamics reacts to the macroscopic scales introduced by the boundary conditions. Both schemes reveal interesting symmetries of scaling, which are reminiscent of the relational interpretation of quantum mechanics and also suggest that the fundamental spatial scale (area gap) may give rise to a temporal scale.

PACS numbers: 04.60.Kz, 04.60.Pp, 98.80.Qc, 03.65.Sq

I. INTRODUCTION

The comprehensive formulation for loop quantum cosmology (LQC, see [1] for a review) in the spatially flat and isotropic model has been constructed in detail [2, 3], giving a conceptual framework and a solid foundation to analyze the physical issues of the quantum theory. With a massless scalar field serving as the *emergent time*, the investigation shows that the quantum evolution is *deterministic across the deep Planck regime* and in the backward evolution of the states which are semiclassical at late times, *the big bang is replaced by a big bounce*.

In the original construction (called “ μ_o -scheme”) of [2, 3], the discreteness variable introduced to impose the fundamental discreteness of quantum geometry is taken to be constant (referred to as μ_o). However, it has been shown that this prescription leads to the wrong semiclassical behavior that, in particular, the critical value of matter density at which the big bounce takes place can be made arbitrarily small by increasing the scalar field momentum p_ϕ . To fix this problem, the construction was further improved by a more sophisticated implementation of the underlying physical ideas of loop quantum gravity (LQG) with the discreteness variable (referred to as $\bar{\mu}$) varying adaptively [4]. In this improved dynamics (called “ $\bar{\mu}$ -scheme”), the big bounce occurs precisely when the matter density enters the Planck regime, regardless of the value of p_ϕ . This construction was also extended to $k = +1$ and $k = -1$ Robertson-Walker models [5, 6].

In order to further develop this formulation and extend its domain of validity, based on the same principles of [2, 3, 4], both the precursor strategy (μ_o -scheme) and

the improved strategy ($\bar{\mu}$ -scheme) were applied and reconstructed for the Bianchi I model to include anisotropy [7]. The analytical investigation shows that the state in the kinematical Hilbert space associated with the classical singularity is *completely decoupled* in the difference evolution equation, indicating that the classical singularity is resolved in the quantum evolution and the big bounce may take place when any of the area scales undergoes the vanishing behavior.

While a thorough numerical investigation for [7] remains to be done to draw the definite conclusion for the details of the quantum evolution in the Bianchi I model, the effective dynamics with LQC discreteness corrections was first studied in [8] using μ_o -scheme for the vacuum solution and the $\bar{\mu}$ -scheme effective dynamics has also been done in [9] for the case with a massless scalar field and in [10] with the inclusion of generic matters. Not only do the results at the level of effective dynamics agree with the anticipations in [7] but more intuitive pictures are also obtained in the semiclassical approach, giving insights into how and why the big bounces take place.

Because of the variety of Bianchi I models, extending the improved scheme is slightly ambiguous as a few strategies are possible. Among them, two schemes are of particular interest (referred to as “ $\bar{\mu}$ -scheme” and “ $\bar{\mu}'$ -scheme” in this paper). The $\bar{\mu}$ -scheme is suggested in [7] and used in [9, 10], while the $\bar{\mu}'$ -scheme is disfavored by [7] and only mentioned briefly in the appendix of [10]. It is later realized that the virtues of $\bar{\mu}'$ -scheme might have been overlooked and we should not dismiss either of them prematurely in favor of the other before more physics is understood, as either scheme has both advantageous and disadvantageous features.

To better understand the difference of their phenomenological ramifications, this paper presents the details of effective dynamics for the Bianchi I model with a massless scalar field in both $\bar{\mu}$ - and $\bar{\mu}'$ -schemes. The investigation shows that in both schemes the big bang

*Electronic address: chiou@gravity.psu.edu

singularity is replaced by the big bounces, which take place *up to three times, once in each diagonal direction*. However, $\bar{\mu}$ - and $\bar{\mu}'$ -schemes give different evolutions, distinct from each other not only in detail but also qualitatively. For instance, the indication of the occurrence of big bounces is the matter density ρ_ϕ in $\bar{\mu}'$ -scheme while it is the “directional density” ϱ_I in $\bar{\mu}$ -scheme. Furthermore, in the different schemes, the big bounces conjoin the different pairs (“antipodal” pair *vs* “conjugate” pair) of classical solutions on the two asymptotic sides of classical regime.

In the Hamiltonian framework, we have to restrict the spatial integration to a finite sized cell \mathcal{V} to make the Hamiltonian finite. This prescription raises the question whether the resulting dynamics is independent of the choice of \mathcal{V} . This issue is very subtle and has caused a great deal of confusion because the dependence on \mathcal{V} of the Ashtekar variables is rather obscure. In order to elucidate the subtleties, the classical dynamics is carefully studied both in metric variables and in Ashtekar variables; the precise physical meanings of Ashtekar variables are then obtained. With the subtleties clarified, it can be shown that the effective dynamics in $\bar{\mu}'$ -scheme is completely independent of the choice of \mathcal{V} as is the classical dynamics, while the effective dynamics in $\bar{\mu}$ -scheme in fact reacts to the macroscopic scales introduced by the boundary conditions of \mathcal{V} . This is an important difference between these two schemes.

In addition to the issues related to the dependence on \mathcal{V} , the effective dynamics in both schemes also reveals other interesting symmetries of scaling, which are reminiscent of the relational interpretation of quantum mechanics. It is also suggested that the fundamental scale (area gap) imposed for the spatial geometry may give rise to a fundamental scale in temporal measurement. These observations could simply be technical artifacts but encourage further investigations for more sophisticated models to tell their profundity.

This paper is organized as follows. In Section II, the classical dynamics of the Bianchi I cosmology with a massless scalar source is solved in Hamiltonian formalism in terms of both metric variables and Ashtekar variables. The effective dynamics with LQC discreteness corrections is constructed and solved in Section III for the $\bar{\mu}$ - and $\bar{\mu}'$ -schemes respectively. The scaling symmetry and issues about relational measurements are discussed in Section IV. Finally, the results and outlooks are summarized in Section V. As a comparison to $\bar{\mu}/\bar{\mu}'$ -scheme, the effective dynamics in μ_o -scheme is also included in Appendix A. The details of heuristic arguments and motivations for $\bar{\mu}$ - and $\bar{\mu}'$ -schemes are given in Appendix B.

II. CLASSICAL DYNAMICS

Before considering the LQC discreteness corrections, in this section, we study the classical dynamics of the Bianchi I cosmology with a massless scalar field. In order

to grasp the precise physical meanings of the Ashtekar variables, which are the fundamental degrees of freedom in LQC, the formulations in metric variables (also see [11]) and in Ashtekar variables are both investigated.

A. Formulation in metric variables

The Hilbert-Einstein action for the cosmology with a massless scalar field ϕ minimally coupled to the gravity is given by

$$\begin{aligned} S &= S_{\text{grav}} + S_\phi := \int d^4x \mathcal{L} := \int dt L \\ &= \frac{1}{16\pi G} \int d^4x \sqrt{-g} R + \frac{1}{2} \int d^4x \sqrt{-g} g^{\mu\nu} \phi_{,\mu} \phi_{,\nu}. \end{aligned} \quad (2.1)$$

In Bianchi I models, the spacetime metric can be written in the diagonal form:

$$\begin{aligned} ds^2 &= g_{\mu\nu} dx^\mu dx^\nu \\ &= -dt^2 + a_1^2(t) dx^2 + a_2^2(t) dy^2 + a_3^2(t) dz^2 \end{aligned} \quad (2.2)$$

and the homogeneous field $\phi(\vec{x}, t) = \phi(t)$ is independent of the spatial coordinates. The temporal variable t is the proper time and a_I are the diagonal scale factors. The coordinates (x, y, z) which diagonalize $g_{\mu\nu}$ are the *co-moving coordinates*.

The metric (2.2) gives the Ricci scalar:

$$R = 2 \left(\frac{\ddot{a}_1}{a_1} + \frac{\ddot{a}_2}{a_2} + \frac{\ddot{a}_3}{a_3} + \frac{\dot{a}_2 \dot{a}_3}{a_2 a_3} + \frac{\dot{a}_1 \dot{a}_3}{a_1 a_3} + \frac{\dot{a}_1 \dot{a}_2}{a_1 a_2} \right). \quad (2.3)$$

This leads to

$$\begin{aligned} S_{\text{grav}} &= \frac{1}{8\pi G} \int d^4x \left\{ \frac{d}{dt} (\dot{a}_1 a_2 a_3 + a_1 \dot{a}_2 a_3 + a_1 a_2 \dot{a}_3) \right. \\ &\quad \left. - a_1 \dot{a}_2 \dot{a}_3 - \dot{a}_1 a_2 \dot{a}_3 - \dot{a}_1 \dot{a}_2 a_3 \right\}. \end{aligned} \quad (2.4)$$

The total time derivative can be ignored and we then have the Lagrangian

$$\begin{aligned} L &= \int d^3x \left\{ -\frac{1}{8\pi G} (a_1 \dot{a}_2 \dot{a}_3 + \dot{a}_1 a_2 \dot{a}_3 + \dot{a}_1 \dot{a}_2 a_3) \right. \\ &\quad \left. + a_1 a_2 a_3 \frac{\dot{\phi}^2}{2} \right\}. \end{aligned} \quad (2.5)$$

Because of homogeneity, the spatial integration diverges as we are considering the noncompact Bianchi I model. To circumvent this problem, the integration is restricted to a finite sized cell \mathcal{V} ; that is, we take

$$\int d^3x \longrightarrow \int_{\mathcal{V}} d^3x = \int_0^{L_1} dx \int_0^{L_2} dy \int_0^{L_3} dz =: V, \quad (2.6)$$

where L_I are the *coordinate* lengths of the edges of \mathcal{V}

and V is its *coordinate* volume.¹ [This prescription is equivalent to compactify the space or impose a spatial periodicity. We will see that this does not change the classical dynamics but might have effect on the quantum corrections.]

With this prescription, the Lagrangian is given by

$$L = V \left\{ -\frac{1}{8\pi G} (a_1 \dot{a}_2 \dot{a}_3 + \dot{a}_1 a_2 \dot{a}_3 + \dot{a}_1 \dot{a}_2 a_3) + a_1 a_2 a_3 \frac{\dot{\phi}^2}{2} \right\} \quad (2.7)$$

and the canonical momenta of ϕ and a_I are defined as:

$$p_\phi := \frac{\partial L}{\partial \dot{\phi}} = V a_1 a_2 a_3 \dot{\phi}, \quad (2.8)$$

$$\pi_1 := \frac{\partial L}{\partial \dot{a}_1} = -\frac{V}{8\pi G} (\dot{a}_2 a_3 + a_2 \dot{a}_3) \quad (2.9)$$

and so on for π_2, π_3 in the cyclic manner.² [Note that the definitions of momenta depend on the cell \mathcal{V} we choose!] Solving (2.9) gives the velocities:

$$\dot{a}_1 = \frac{4\pi G}{V} \left(\frac{a_1 \pi_1}{a_2 a_3} - \frac{\pi_2}{a_3} - \frac{\pi_3}{a_2} \right), \quad (2.10)$$

by which we find the Hamiltonian:

$$\begin{aligned} H &:= \pi_1 \dot{a}_1 + \pi_2 \dot{a}_2 + \pi_3 \dot{a}_3 + p_\phi \dot{\phi} - L \\ &= V^{-1} \left\{ 2\pi G \left[-\frac{2\pi_2 \pi_3}{a_1} - \frac{2\pi_1 \pi_3}{a_2} - \frac{2\pi_1 \pi_2}{a_3} \right. \right. \\ &\quad \left. \left. + \frac{a_1 \pi_1^2}{a_2 a_3} + \frac{a_2 \pi_2^2}{a_1 a_3} + \frac{a_3 \pi_3^2}{a_1 a_2} \right] + \frac{p_\phi^2}{2a_1 a_2 a_3} \right\} \end{aligned} \quad (2.11)$$

with the canonical relations:

$$\{\phi, p_\phi\} = 1, \quad (2.12)$$

$$\{a_I, \pi_J\} = \delta_{IJ}. \quad (2.13)$$

We can simplify the Hamiltonian by choosing the lapse function $N = V a_1 a_2 a_3$ and thus introducing the new time variable $dt' = (V a_1 a_2 a_3)^{-1} dt$. The rescaled Hamiltonian is then given by

$$\begin{aligned} H' &= 2\pi G (-2a_2 a_3 \pi_2 \pi_3 - 2a_1 a_3 \pi_1 \pi_3 - 2a_1 a_2 \pi_1 \pi_2 \\ &\quad + a_1^2 \pi_1^2 + a_2^2 \pi_2^2 + a_3^2 \pi_3^2) + \frac{p_\phi^2}{2}. \end{aligned} \quad (2.14)$$

The equations of motion are governed by the Hamilton's equations:

$$\frac{dp_\phi}{dt'} = \{p_\phi, H'\} = 0 \Rightarrow p_\phi \text{ is constant}, \quad (2.15)$$

$$\frac{d\phi}{dt'} = \{\phi, H'\} = p_\phi, \quad (2.16)$$

$$\begin{aligned} \frac{da_1}{dt'} &= \{a_1, H'\} = \frac{\partial H'}{\partial \pi_1} \\ &= 4\pi G a_1 (a_1 \pi_1 - a_2 \pi_2 - a_3 \pi_3), \end{aligned} \quad (2.17)$$

$$\begin{aligned} \frac{d\pi_1}{dt'} &= \{\pi_1, H'\} = -\frac{\partial H'}{\partial a_1} \\ &= -4\pi G \pi_1 (a_1 \pi_1 - a_2 \pi_2 - a_3 \pi_3). \end{aligned} \quad (2.18)$$

In addition, the Hamiltonian must vanish:

$$H'(a_I, \pi_I, p_\phi) = 0. \quad (2.19)$$

Combining (2.17) and (2.18) gives

$$\frac{d}{dt'} (a_I \pi_I) = 0. \quad (2.20)$$

We assign

$$a_1 \pi_1 = -\hbar (\mathcal{K}_2 + \mathcal{K}_3) \quad (2.21)$$

with the dimensionless constants \mathcal{K}_I , which will be used to parameterize the solutions of evolution. Equations (2.16) and (2.17) then give

$$\frac{1}{a_I} \frac{da_I}{d\phi} = 8\pi G \hbar \frac{\mathcal{K}_I}{p_\phi} = \sqrt{8\pi G} \frac{\mathcal{K}_I}{\mathcal{K}_\phi}, \quad (2.22)$$

if we define

$$p_\phi := \hbar \sqrt{8\pi G} \mathcal{K}_\phi \quad (2.23)$$

with the dimensionless constant \mathcal{K}_ϕ . Regarding ϕ as the *emergent time*, the solutions of evolution are given by

$$a_I(\phi) = a_I(\phi_0) e^{\sqrt{8\pi G} \frac{\kappa_I}{\mathcal{K}_\phi} (\phi - \phi_0)}, \quad (2.24)$$

where we scale the parameters $\mathcal{K}_I = \mathcal{K} \kappa_I$, $\mathcal{K}_\phi = \mathcal{K} \kappa_\phi$ (with $\mathcal{K} > 0$) such that

$$\kappa_1 + \kappa_2 + \kappa_3 = \pm 1. \quad (2.25)$$

The Hamiltonian constraint (2.19) now reads as

$$\mathcal{K}_\phi^2 = 2 (\mathcal{K}_2 \mathcal{K}_3 + \mathcal{K}_1 \mathcal{K}_3 + \mathcal{K}_1 \mathcal{K}_2) \quad (2.26)$$

or equivalently

$$\kappa_1^2 + \kappa_2^2 + \kappa_3^2 + \kappa_\phi^2 = 1. \quad (2.27)$$

¹ The *coordinate* lengths L_I and volume V are independent of time once the cell \mathcal{V} is chosen since we are working on the *co-moving coordinates*. The *physical* lengths of the edges and volume of \mathcal{V} are given by $\mathbf{L}_I := a_I L_I$ and $\mathbf{V} := a_1 a_2 a_3 V$ respectively, which evolve with time.

² We will not mention the obvious cyclic repetition hereafter.

The classical Bianchi I model with a massless scalar field admits both “Kasner-like” (two of κ_I positive/negative and the other negative/positive) and “Kasner-unlike” (all κ_I positive/negative) solutions. The Kasner-like solution, which has two expanding and one

contracting directions (say, $\kappa_\phi > 0$ and $\kappa_1 + \kappa_2 + \kappa_3 = 1$), eventually encounters the “Kasner-like singularity” (a given regular cubical cell stretches as an infinitely long line) in the far past and the “planar collapse” (a regular cubical cell stretches as an infinitely large plane) in the far future. On the other hand, the Kasner-unlike solution, with all directions expanding, encounters the “Kasner-unlike singularity” (a regular cubical cell vanishes to a point) in the far past and no planar collapse.³

We will see that with LQC discreteness corrections, both Kasner-like and Kasner-unlike singularities are resolved and replaced by the *big bounces*, whereas the planar collapse remains its destiny even one of the three diagonal directions approaches infinitely small length scale.

Note that, by (2.8) and (2.9), p_ϕ and π_I depend on the choice of \mathcal{V} and scale as $p_\phi, \pi_I \propto V$. Thus, the directly measurable quantities are not the canonical momenta but rather the momentum density of ϕ :

$$\frac{p_\phi}{V} \equiv \dot{\phi} = \mathbf{V}^{-1} \hbar \sqrt{8\pi G} \mathcal{K}_\phi, \quad (2.30)$$

which is nothing but the time derivative of ϕ , and the quantities:

$$\frac{a_1 \pi_1}{V} \equiv -\frac{1}{2\pi G} (H_2 + H_3) = -\frac{\hbar}{V} (\mathcal{K}_2 + \mathcal{K}_3) \quad (2.31)$$

with the *directional Hubble rates* defined as

$$H_I := \frac{\dot{a}_I}{a_I} = \frac{\dot{\mathbf{L}}_I}{\mathbf{L}_I}. \quad (2.32)$$

For given initial physical conditions $\dot{\phi}|_{t_0}$ and $H_I|_{t_0}$, the constants of motion \mathcal{K}_ϕ and \mathcal{K}_I both scale as $\propto V|_{t_0}$, the physical volume of \mathcal{V} at the initial time t_0 . The ratio $\mathcal{K}_I/\mathcal{K}_\phi = \kappa_I/\kappa_\phi$ is nevertheless independent of \mathcal{V} and hence the solution of $a_I(\phi)$ given by (2.24) does *not* depend on the choice of \mathcal{V} . Once $a_I(\phi)$ is solved, to know the solution $a_I(t)$ as a function of t , we only need to convert ϕ back to t via

$$\begin{aligned} t - t_0 &= \int_{t_0}^t dt = \int_{\phi_0}^\phi \frac{V a_1(\phi) a_2(\phi) a_3(\phi)}{p_\phi} d\phi \\ &= \int_{\phi_0}^\phi \frac{a_1(\phi) a_2(\phi) a_3(\phi)}{a_1(\phi_0) a_2(\phi_0) a_3(\phi_0) \dot{\phi}|_{t_0}} d\phi, \end{aligned} \quad (2.33)$$

³ In the case of no matter sources, the classical dynamics of vacuum Bianchi I model yields the standard *Kasner solution*:

$$a_I(t) = a_I(t_0) \left(\frac{t}{t_0} \right)^{\kappa_I}, \quad (2.28)$$

where $\kappa_1, \kappa_2, \kappa_3$ are constants subject to:

$$\kappa_1 + \kappa_2 + \kappa_3 = 1 \quad \text{and} \quad \kappa_1^2 + \kappa_2^2 + \kappa_3^2 = 1, \quad (2.29)$$

which are to be compared with (2.25) and (2.27). Apart from the trivial solution (where two of κ_I vanish), all Kasner solutions must have two of κ_I positive and the other negative.

where, again, the dependence of V is gone. Therefore, whether in terms of the proper time t or the emergent time ϕ , the classical dynamics is *completely independent* of the finite sized cell \mathcal{V} we choose to make sense of the Hamiltonian formalism. [The independence of the choice of \mathcal{V} is not necessarily retained when quantum corrections are taken into account. In any case, however, the dynamics is independent of \mathcal{V} in terms of t if and only if it is so in terms of ϕ .] Furthermore, (2.33) gives a simple relation:

$$t - t_0 = \frac{\kappa_\phi}{\sqrt{8\pi G} \dot{\phi}|_{t_0}} \left(e^{\frac{\sqrt{8\pi G}}{\kappa_\phi} (\phi - \phi_0)} - 1 \right) \quad (2.34)$$

for the classical solutions given by (2.24), but the relation between t and ϕ is more complicated if the quantum corrections are taken into account.

B. Formulation in Ashtekar variables

Equivalently, the classical dynamics studied above can be reformulated in terms of Ashtekar variables as the groundwork for LQC formulation. We follow the lines of Section III of [7] but emphasize the explicit relations between the metric and Ashtekar variables by rigorously taking care of the subtleties overlooked (and correcting the mistakes made) in [7, 9].

In Bianchi (homogeneous) models of cosmology, on the homogeneous space-like slice Σ , we can choose a fiducial triad of vectors ${}^o e_i^a$ and a fiducial co-triad of covectors ${}^o \omega_a^i$ that are left invariant by the action of the Killing fields of Σ . (Note ${}^o e_i^a {}^o \omega_b^i = \delta_b^a$.) The *fiducial* 3-metric of Σ is given by the co-triad ${}^o \omega_a^i$:

$${}^o q_{ab} = {}^o \omega_a^i {}^o \omega_b^j \delta_{ij}. \quad (2.35)$$

In LQG, the Ashtekar variables consist of the canonical pairs: the densitized triads $\tilde{E}^a_i(\vec{x})$ and connections $A_a^i(\vec{x})$, which satisfy the canonical relation:

$$\{A_a^i(\vec{x}), \tilde{E}^b_j(\vec{x}')\} = 8\pi G \gamma \delta_j^i \delta_a^b \delta^3(\vec{x} - \vec{x}'), \quad (2.36)$$

where γ is the Barbero-Immirzi parameter. In the context of Bianchi models, it is more convenient to consider the *reduced canonical variables*:

$$\begin{aligned} E^i_j &:= \int_{\mathcal{V}} d^3x \sqrt{q} \left({}^o q^{-1/2} {}^o \omega_a^i \tilde{E}^a_j \right) \\ &= \int_{\mathcal{V}} d^3x {}^o \omega_a^i \tilde{E}^a_j, \end{aligned} \quad (2.37)$$

$$A_i^j := \int_{\mathcal{V}} d^3x \sqrt{q} (A_a^j {}^o e_i^a). \quad (2.38)$$

The reduced canonical variables are essentially the same as the original canonical variables, but stripped of the spatial dependence enforced by the Bianchi symmetry

and integrated over a finite sized cell \mathcal{V} .⁴ Conversely, we have the replacement rules:

$$\tilde{E}^a_i \longrightarrow V_o^{-1} \sqrt{q} E^j_i e^a_j = V^{-1} E^j_i e^a_j, \quad (2.39)$$

$$A_a^i \longrightarrow V_o^{-1} A_j^i \omega_a^j, \quad (2.40)$$

where V_o is the *fiducial* volume defined as the volume of \mathcal{V} measured as if the 3-metric was ${}^oq_{ab}$, i.e.

$$V_o := \int_{\mathcal{V}} d^3x \sqrt{{}^oq}. \quad (2.41)$$

The canonical relation (2.36) now reads as

$$\{A_i^j, E^k_l\} = 8\pi G \gamma V_o \delta_i^k \delta_l^j. \quad (2.42)$$

However, if we compute $\{A_a^i, \tilde{E}^b_j\}$ using (2.39) and (2.40) through (2.42), the δ -function in the right hand side of (2.36) is correspondingly replaced with

$$\delta^3(\vec{x} - \vec{x}') \longrightarrow V^{-1} \quad (2.43)$$

as expected due to the regularization procedure.

For the diagonal Bianchi class A models (Bianchi I included), E^i_j and A_i^j are diagonalizable and their diagonalized entries are denoted as \tilde{p}_I and \tilde{c}_I ($I = 1, 2, 3$) respectively. Equation (2.42) then becomes

$$\{\tilde{c}_I, \tilde{p}_J\} = 8\pi G \gamma V_o \delta_{IJ}. \quad (2.44)$$

In Bianchi I models, correspondingly, we choose the fiducial 3-metric to be the diagonal form:

$${}^oq_{ab} = \begin{pmatrix} {}^o a_1^2 & 0 & 0 \\ 0 & {}^o a_2^2 & 0 \\ 0 & 0 & {}^o a_3^2 \end{pmatrix}, \quad (2.45)$$

and the finite sized cell \mathcal{V} is adapted to be rectangular with respect to ${}^oq_{ab}$ and coordinated as described in (2.6). The fiducial volume of \mathcal{V} is now $V_o = {}^o L_1 {}^o L_2 {}^o L_3 = {}^o a_1 {}^o a_2 {}^o a_3 V$ with

$${}^o L_I := \int_0^{L_I} {}^o a_I dx_I = {}^o a_I L_I \quad (2.46)$$

being the *fiducial* lengths of the edges of \mathcal{V} .⁵

To get rid of the nonphysical dependence on ${}^oq_{ab}$, it is convenient to introduce the new variables:

$$p_I := {}^o L_I^{-1} \tilde{p}_I, \quad (2.47)$$

$$c_1 := ({}^o L_2 {}^o L_3)^{-1} \tilde{c}_1, \quad (2.48)$$

which satisfy the canonical relation:

$$\{c_I, p_J\} = 8\pi G \gamma \delta_{IJ}. \quad (2.49)$$

The relation between the densitized triad and the 3-metric is given by

$$qq^{ab} = \delta^{ij} \tilde{E}^a_i \tilde{E}^b_j, \quad (2.50)$$

which leads to

$$p_1 = L_2 L_3 (a_2 a_3) = \mathbf{L}_2 \mathbf{L}_3. \quad (2.51)$$

Thus, the triad variables p_I are the *physical* areas of the rectangular surfaces of \mathcal{V} .⁶ Comparing the canonical relations (2.13) and (2.49) via (2.51), we have

$$c_1 = \frac{4\pi\gamma G}{L_2 L_3 a_2 a_3} (a_1 \pi_1 - a_2 \pi_2 - a_3 \pi_3). \quad (2.52)$$

By (2.9), we have

$$c_I = \gamma L_I \dot{a}_I = \gamma \mathbf{L}_I H_I = \gamma \dot{\mathbf{L}}_I, \quad (2.53)$$

which tells that, *classically*, the connection variables c_I are the time change rates of the *physical* lengths of the edges of \mathcal{V} (up to the constant γ). Note that (2.51) and (2.52) remain the same even with the quantum corrections since the symplectic structures given by (2.13) and (2.49) as well as the relation (2.50) are unchanged. By contrast, (2.53) is modified in the presence of quantum effects because Hamiltonian is changed and thus (2.9) no longer holds.

By (2.51) and (2.52), the classical Hamiltonian (2.11) can be recast in terms of c_I and p_I :

$$\begin{aligned} H &= H_{\text{grav}} + H_{\phi} \\ &= -\frac{(c_2 p_2 c_3 p_3 + c_1 p_1 c_3 p_3 + c_1 p_1 c_2 p_2)}{8\pi G \gamma^2 \sqrt{p_1 p_2 p_3}} + \frac{p_{\phi}^2}{2\sqrt{p_1 p_2 p_3}}. \end{aligned} \quad (2.54)$$

[We can also derive H_{grav} directly from the Hamiltonian constraint of the full theory of LQG. For this approach, see the text toward (B4) in Appendix B or Section III.C of [7].] The solutions of c_I and p_I can be readily obtained by translating (2.21) and (2.24) via (2.51) and (2.52). But in order to draw a parallel to solving the effective dynamics with LQC corrections studied later, in the following, we present solving the equations of motions directly for c_I and p_I .

⁴ The spatial integration over a finite sized cell \mathcal{V} is not explicitly noted in [7] and nor in most literatures. This prescription is subtle but important because otherwise the Poisson bracket $\{E^i_j, A_i^j\}$ would be distributional.

⁵ The *fiducial* length/volume should not be confused with the *coordinate* or *physical* length/volume (see Footnote 1). (Also note: V_o and ${}^o L_I$ could depend on t , depending on the choice of ${}^o q_{ab}$.) Most literatures do not distinguish these notions completely, but the nuances are highlighted in this paper in order to give the precise physical interpretations of c_I and p_I .

⁶ More precisely, (2.51) should be $|p_I| = \mathbf{L}_2 \mathbf{L}_3$. The sign of p_I corresponds to spatial orientation, which we ignore in this paper.

Again, we simplify the Hamiltonian by choosing the lapse function $N = \sqrt{p_1 p_2 p_3} = V a_1 a_2 a_3$ and thus introducing the new time variable $dt' = (p_1 p_2 p_3)^{-1/2} dt = (V a_1 a_2 a_3)^{-1} dt$. The rescaled Hamiltonian (which is the same as (2.14)) is given by

$$H' = -\frac{(c_2 p_2 c_3 p_3 + c_1 p_1 c_3 p_3 + c_1 p_1 c_2 p_2)}{8\pi G \gamma^2} + \frac{p_\phi^2}{2}. \quad (2.55)$$

The equations of motion are governed by (2.15) and (2.16) as well as

$$\begin{aligned} \frac{dc_1}{dt'} &= \{c_1, H'\} = 8\pi G \gamma \frac{\partial H'}{\partial p_1} \\ &= -\gamma^{-1} c_1 (c_2 p_2 + c_3 p_3), \end{aligned} \quad (2.56)$$

$$\begin{aligned} \frac{dp_1}{dt'} &= \{p_1, H'\} = -8\pi G \gamma \frac{\partial H'}{\partial c_1} \\ &= \gamma^{-1} p_1 (c_2 p_2 + c_3 p_3). \end{aligned} \quad (2.57)$$

In addition, the constraint that the Hamiltonian must vanish yields

$$\begin{aligned} H'(c_I, p_I, p_\phi) &= 0 \quad \Rightarrow \\ p_\phi^2 &= \frac{1}{4\pi G \gamma^2} (c_2 p_2 c_3 p_3 + c_1 p_1 c_3 p_3 + c_1 p_1 c_2 p_2). \end{aligned} \quad (2.58)$$

[Note that substituting (2.51) into (2.57) leads to (2.53) again.]

Combining (2.56) and (2.57) gives

$$\frac{d}{dt'}(p_I c_I) = 0, \quad \Rightarrow \quad p_I c_I = 8\pi G \gamma \hbar \mathcal{K}_I, \quad (2.59)$$

where \mathcal{K}_I are the same constants as defined in (2.21). Taking (2.59) into (2.58) yields the same constraint (2.26).

Putting (2.59) into (2.57) gives

$$\frac{1}{p_1} \frac{dp_1}{dt'} = 8\pi G \hbar (\mathcal{K}_2 + \mathcal{K}_3). \quad (2.60)$$

Referring to (2.16), this leads to

$$\frac{1}{p_1} \frac{dp_1}{d\phi} = 8\pi G \hbar \frac{\mathcal{K}_2 + \mathcal{K}_3}{p_\phi} = \sqrt{8\pi G} \left(\frac{1 - \kappa_I}{\kappa_\phi} \right), \quad (2.61)$$

and consequently

$$p_I(\phi) = p_I(\phi_0) e^{\sqrt{8\pi G} \left(\frac{1 - \kappa_I}{\kappa_\phi} \right) (\phi - \phi_0)}, \quad (2.62)$$

which is the same solution as given by (2.24).

III. EFFECTIVE DYNAMICS WITH LQC DISCRETENESS CORRECTIONS

In LQC, the connection variables c_I do not exist and should be replaced with holonomies. In the effective theory, to capture the quantum corrections, following the

procedures used in the isotropic case [12], we take the prescription to replace c_I with

$$c_I \longrightarrow \frac{\sin(\bar{\mu}_I c_I)}{\bar{\mu}_I}, \quad (3.1)$$

introducing the discreteness variables $\bar{\mu}_I$. The heuristic argument starting from the full theory of LQG and leading to (3.1) can be found in Appendix B. This prescription can also be understood as the WKB approximation of the full quantum theory of LQC [8].

Imposing this prescription plus the loop quantum correction to the inverse triad on (2.54), we have the effective Hamiltonian constraint to the leading order:

$$\begin{aligned} H_{\text{eff}} &= f(p_1) f(p_2) f(p_3) \frac{p_\phi^2}{2} - \frac{f(p_1) f(p_2) f(p_3)}{8\pi G \gamma^2} \\ &\quad \times \left\{ \frac{\sin(\bar{\mu}_2 c_2) \sin(\bar{\mu}_3 c_3)}{\bar{\mu}_2 \bar{\mu}_3} p_2 p_3 + \text{cyclic terms} \right\}, \end{aligned} \quad (3.2)$$

where $f(p_I)$ is the eigenvalue of the inverse triad operator $1/\sqrt{p_I}$. The loop quantization gives the quantum corrections on $f(p_I)$:

$$f(p_I) \sim \begin{cases} \frac{1}{\sqrt{p_I}} (1 + \mathcal{O}(\ell_{\text{Pl}}^2/p_I)) & \text{for } p_I \gg \ell_{\text{Pl}}^2 \\ \propto p_I^n / \ell_{\text{Pl}}^{2n+1} & \text{for } p_I \ll \ell_{\text{Pl}}^2 \end{cases} \quad (3.3)$$

with the Planck length $\ell_{\text{Pl}} := \sqrt{G\hbar}$ and a positive n . The corrections to $f(p_I)$ are significant only in the deep Planck regime in the vicinity of $p_I = 0$. From now on, we will ignore the quantum corrections to $f(p_I)$ by simply taking its classical function $f(p_I) = p_I^{-1/2}$. The fact that this effective quantum modification is a good approximation for the sates which are semiclassical at late times has been verified in the isotropic models of LQC sourced with a massless scalar field [4, 13]. The validity of this effective prescription for the vacuum Bianchi I model was discussed in the context of WKB approximation in [8] and that for the Bianchi I model with a massless scalar field can also be affirmed [14]. [We will see that in the backward evolution of the solutions which are semiclassical in the late times, the big bounces take place much earlier before the discreteness correction on the inverse triad operator becomes considerable, and it is the “non-locality” effect (i.e., using the holonomies) that accounts for the occurrence of big bounces.]

With $f(p_I) = p_I^{-1/2}$, by choosing $N = \sqrt{p_a p_2 p_3}$ and $dt' = (p_1 p_2 p_3)^{-1/2} dt$, the Hamiltonian (3.2) can be rescaled as

$$\begin{aligned} H'_\mu &= \frac{p_\phi^2}{2} \\ &\quad - \frac{1}{8\pi G \gamma^2} \left\{ \frac{\sin(\bar{\mu}_2 c_2) \sin(\bar{\mu}_3 c_3)}{\bar{\mu}_2 \bar{\mu}_3} p_2 p_3 + \text{cyclic terms} \right\}. \end{aligned} \quad (3.4)$$

As for imposing the fundamental discreteness of LQC on the formulation of LQC, the precursor construction (μ_o -scheme) is to take $\bar{\mu}_I$ as constants (referred to as μ_μ^o).

However, it has been shown that in the isotropic case μ_o -scheme can lead to the wrong semiclassical limit and should be improved by a more sophisticated construction ($\bar{\mu}$ -scheme) in which the value of $\bar{\mu}$ depends adaptively on p (via $\bar{\mu} \propto 1/\sqrt{p}$) and thus implements the underlying physics of quantum geometry of LQG more directly [4]. Extending this scheme to the Bianchi I model is slightly ambiguous as a few possibilities exist. Among them, two constructions are most preferable (referred to as “ $\bar{\mu}$ -scheme” and “ $\bar{\mu}'$ -scheme”):

- $\bar{\mu}$ -scheme:

$$\bar{\mu}_1 = \sqrt{\frac{\Delta}{p_1}}, \quad \bar{\mu}_2 = \sqrt{\frac{\Delta}{p_2}}, \quad \bar{\mu}_3 = \sqrt{\frac{\Delta}{p_3}}, \quad (3.5)$$

- $\bar{\mu}'$ -scheme:

$$\bar{\mu}'_1 = \sqrt{\frac{p_1 \Delta}{p_2 p_3}}, \quad \bar{\mu}'_2 = \sqrt{\frac{p_2 \Delta}{p_1 p_3}}, \quad \bar{\mu}'_3 = \sqrt{\frac{p_3 \Delta}{p_1 p_2}}. \quad (3.6)$$

Here $\Delta = \frac{\sqrt{3}}{2}(4\pi\gamma\ell_{\text{Pl}}^2)$ is the *area gap* in the full theory of LQG.

Either scheme has its own advantages and drawbacks and until more detailed physics is investigated it is still debatable which one makes better sense. In particular, $\bar{\mu}$ -scheme is suggested in [7], since in the construction for the full theory of LQC the Hamiltonian constraint in $\bar{\mu}$ -scheme gives a difference equation in terms of affine variables and therefore the well-developed framework of the spatially flat-isotropic LQC can be straightforwardly adopted. (However, it is argued in [15] that $\bar{\mu}$ -scheme may lead to an unstable difference equation.) By contrast, $\bar{\mu}'$ -scheme does not admit the required affine variables and the full LQC of it is very difficult to construct. On the other hand, $\bar{\mu}'$ -scheme has the virtue that its effective dynamics is independent of the choice of \mathcal{V} as will be seen. (More detailed comparisons and the heuristic arguments for both schemes are presented in Appendix B.) To explore their differences, we study both $\bar{\mu}$ -scheme and $\bar{\mu}'$ -scheme in the context of effective dynamics in Section III A and Section III B respectively. (As a comparison, the effective dynamics in μ_o -scheme is also presented in Appendix A, where we see the insensible behavior that p_I can be made arbitrarily small.)

A. Effective dynamics in $\bar{\mu}$ -scheme

The effective dynamics in $\bar{\mu}$ -scheme is specified by the Hamiltonian (3.4) with $\bar{\mu}_I$ given by (3.5). Again, the equations of motion are governed by the Hamilton's equations and the constraint that the Hamiltonian must vanish:

$$\frac{dp_\phi}{dt'} = \{p_\phi, H'_\mu\} = 0 \quad \Rightarrow \quad p_\phi \text{ is constant}, \quad (3.7)$$

$$\frac{d\phi}{dt'} = \{\phi, H'_\mu\} = p_\phi, \quad (3.8)$$

$$\begin{aligned} \frac{dc_1}{dt'} &= \{c_1, H'_\mu\} = 8\pi G\gamma \frac{\partial H'_\mu}{\partial p_1} \\ &= -\gamma^{-1} \left[\frac{3 \sin(\bar{\mu}_1 c_1)}{2\bar{\mu}_1} - \frac{c_1 \cos(\bar{\mu}_1 c_1)}{2} \right] \\ &\quad \times \left[\frac{\sin(\bar{\mu}_2 c_2)}{\bar{\mu}_2} p_2 + \frac{\sin(\bar{\mu}_3 c_3)}{\bar{\mu}_3} p_3 \right], \end{aligned} \quad (3.9)$$

$$\begin{aligned} \frac{dp_1}{dt'} &= \{p_1, H'_\mu\} = -8\pi G\gamma \frac{\partial H'_\mu}{\partial c_1} \\ &= \gamma^{-1} p_1 \cos(\bar{\mu}_1 c_1) \\ &\quad \times \left[\frac{\sin(\bar{\mu}_2 c_2)}{\bar{\mu}_2} p_2 + \frac{\sin(\bar{\mu}_3 c_3)}{\bar{\mu}_3} p_3 \right], \end{aligned} \quad (3.10)$$

as well as

$$\begin{aligned} H'_\mu(c_I, p_I, p_\phi) &= 0 \quad \Rightarrow \quad p_\phi^2 = \\ &\frac{1}{4\pi G\gamma^2} \left\{ \frac{\sin(\bar{\mu}_2 c_2) \sin(\bar{\mu}_3 c_3)}{\bar{\mu}_2 \bar{\mu}_3} p_2 p_3 + \text{cyclic terms} \right\}. \end{aligned} \quad (3.11)$$

[Note that in the classical limit $\bar{\mu}_I c_I \rightarrow 0$, we have $\sin(\bar{\mu}_I c_I)/\bar{\mu}_I \rightarrow c_I$, $\cos(\bar{\mu}_I c_I) \rightarrow 1$ and therefore (3.9)–(3.11) reduce to their classical counterparts (2.56)–(2.58).] Also notice that substituting (2.51) into (3.10) gives

$$\begin{aligned} &\frac{\sin(\bar{\mu}_1 c_1)}{\bar{\mu}_1} \\ &= \frac{\gamma \mathbf{L}_1}{2} \left\{ \frac{H_1 + H_3}{\cos(\bar{\mu}_2 c_2)} + \frac{H_1 + H_2}{\cos(\bar{\mu}_3 c_3)} - \frac{H_2 + H_3}{\cos(\bar{\mu}_1 c_1)} \right\}, \end{aligned} \quad (3.12)$$

which is the modification of (2.53) with quantum corrections.

Combining (3.9) and (3.10), we have

$$\begin{aligned} &\left(\frac{3 \sin(\bar{\mu}_I c_I)}{2\bar{\mu}_I} - \frac{c_I \cos(\bar{\mu}_I c_I)}{2} \right) \frac{dp_I}{dt'} + p_I \cos(\bar{\mu}_I c_I) \frac{dc_I}{dt'} \\ &= \frac{d}{dt'} \left[p_I \frac{\sin(\bar{\mu}_I c_I)}{\bar{\mu}_I} \right] = 0, \end{aligned} \quad (3.13)$$

which, in accordance with the classical counterpart (2.59), yields

$$p_I \frac{\sin(\bar{\mu}_I c_I)}{\bar{\mu}_I} = 8\pi G\gamma \hbar \mathcal{K}_I. \quad (3.14)$$

Taking (3.14) into (3.11) again gives the same constraints on the constant parameters as in (2.26).

Substituting (3.14) into (3.10) yields

$$\frac{1}{p_1} \frac{dp_1}{dt'} = 8\pi G\hbar \cos(\bar{\mu}_1 c_1) (\mathcal{K}_2 + \mathcal{K}_3). \quad (3.15)$$

By regarding ϕ as the emergent time via (3.8) and expressing $\cos x = \pm \sqrt{1 - \sin^2 x}$, (3.15) then leads to

$$\frac{1}{p_I} \frac{dp_I}{d\phi} = \pm \sqrt{8\pi G} \left(\frac{1 - \kappa_I}{\kappa_\phi} \right) \left[1 - \frac{\varrho_I}{\varrho_{I, \text{crit}}} \right]^{1/2}, \quad (3.16)$$

where we define the *directional density* for the I -direction:

$$\varrho_I := \frac{p_\phi^2}{p_I^3} \quad (3.17)$$

and its critical value is given by the *Planckian density* ρ_{Pl} times a numerical factor κ_ϕ^2/κ_I^2 :

$$\varrho_{I,\text{crit}} := \left(\frac{\kappa_\phi}{\kappa_I}\right)^2 \rho_{\text{Pl}}, \quad \rho_{\text{Pl}} := (8\pi G\gamma^2 \Delta)^{-1}. \quad (3.18)$$

[Note that the directional density ϱ_I is of the same dimension as the matter density $\rho_\phi := p_\phi^2/(2p_1p_2p_3)$ and thus the name.]

From (3.16), we conclude: The big bang singularity (whether Kasner-like or Kasner-unlike) is *replaced by the big bounces*, which take place up to three times, once in each direction whenever each of ϱ_I approaches its critical value $\varrho_{I,\text{crit}}$ (and thus $\cos(\bar{\mu}_I c_I)$ flips sign in (3.15)). Furthermore, the differential equations of individual p_I are *completely decoupled* from one another and as a result the epochs of the big bounces in different directions can be arbitrarily separate, depending on the given initial condition. Also notice that the constants κ_I remain the same before and after the bounces. Equivalently, it can be rephrased that the big bounces connect the classical solution specified by $\kappa_1, \kappa_2, \kappa_3$ on one asymptotic side with its “antipodal” counterpart on the other asymptotic side specified by the “antipodal” parameters:

$$\kappa_1, \kappa_2, \kappa_3 \longleftrightarrow -\kappa_1, -\kappa_2, -\kappa_3. \quad (3.19)$$

On the other hand, however, the planar collapse in the Kasner-like case is *not* resolved but the vanishing behavior of one of the length scale factors a_I continues.

For given initial conditions, the differential equation (3.16) can be solved numerically.⁷ The evolutions of $p_I(\phi)$, $a_I(\phi)$ and $\varrho_I(\phi)$ are depicted in parts (a), (b) and (c) respectively in FIG. 1 for Kasner-unlike solution and in FIG. 2 for Kasner-like solution. Note that the bounces occur at the moments exactly when ϱ_I approach their critical values. Also notice that each individual curve of $p_I(\phi)$ and $a_I(\phi)$ in logarithmic scale becomes a straight line before and after the bounce, with the same slope but opposite sign, indicating that the bounces conjoin the two antipodal classical solutions.

It is noteworthy that the directional density ϱ_I is the indication of the bounces but the quantity of ϱ_I is *not* independent of the choice of \mathcal{V} , as we know

$$\varrho_1 = \frac{p_\phi^2}{p_1^3} = \frac{\mathbf{V}^2 \dot{\phi}^2}{\mathbf{L}_2^2 \mathbf{L}_3^2} = \frac{\mathbf{L}_1^2}{\mathbf{L}_2 \mathbf{L}_3} \dot{\phi}^2 \quad (3.20)$$

⁷ Equivalently, we can directly solve the coupled differential equations (3.8)–(3.10) for given $p_I(\phi_0)$, $c_I(\phi_0)$ and p_ϕ . Also note that, to give the initial condition, an alternative way is to specify $p_I(\phi_0)$ together with the constants \mathcal{K}_I and \mathcal{K}_ϕ . Given $p_I(\phi_0)$ and \mathcal{K}_I , $c_I(\phi_0)$ are fixed by (3.14).

by (2.30) and (2.51). Therefore, contrast to the classical dynamics, the effective dynamics in $\bar{\mu}$ -scheme does *depend* on the choice of the finite sized cell \mathcal{V} . Another subtler dependence on \mathcal{V} comes from the fact that for given initial physical conditions $\dot{\phi}|_{t_0}$ and $H_I|_{t_0}$, the constant of motion \mathcal{K}_ϕ scale as $\propto \mathbf{V}|_{t_0}$ but \mathcal{K}_I scale as $\propto \mathbf{V}|_{t_0}$ only approximately (see (3.12) and (3.14) and notice (3.12) involves the quantum modification with terms $\cos(\bar{\mu}_I c_I)$). As a result, the ratio $\mathcal{K}_\phi/\mathcal{K}_I = \kappa_\phi/\kappa_I$ is slightly dependent on \mathcal{V} . (Nevertheless, in the classical regime, we still have $\kappa_\phi/\kappa_I \approx (8\pi G)^{1/2} \dot{\phi}/H_I$.)

The problem not to be invariant under different choice of \mathcal{V} is absent in the $\bar{\mu}'$ -scheme as will be seen in Section III B. However, we should not dismiss $\bar{\mu}$ -scheme immediately as it is a common phenomenon that a quantum system reacts to macroscopic scales introduced by boundary conditions (for instance, the well-known “conformal anomaly” as a “soft” breaking of conformal symmetry). If we have good physical input to tell what exactly the space is to be enclosed as \mathcal{V} (such as in the compactified Bianchi I model, or applied for the finite sized homogeneous patches in the Belinsky-Khalatnikov-Lifshitz (BKL) scenario), the dependence on \mathcal{V} could be rather meritorious than problematic and the bounce occurrence condition ($\varrho_I = \varrho_{I,\text{crit}}$) can be understood as: The *physical areas* ($p_1 = \mathbf{L}_2 \mathbf{L}_3$, etc) of the surfaces of \mathcal{V} get bounced when each of them undergoes the Planck regime (times a numerical value κ_I^2/κ_ϕ^2) measured by the reference of the momentum p_ϕ .

B. Effective dynamics in $\bar{\mu}'$ -scheme

The effective dynamics in $\bar{\mu}$ -scheme is specified by the Hamiltonian (3.4) with $\bar{\mu}_I$ replaced by $\bar{\mu}'_I$ given in (3.6). For simplicity, we choose a different lapse function $N = (p_1 p_2 p_3)^{-1/2}$ and correspondingly introduce the new time variable $dt'' = (p_1 p_2 p_3)^{1/2} dt$. With the new lapse, the Hamiltonian (3.4) is further rescaled to the simpler form:

$$H''_{\bar{\mu}'} = \rho_\phi - \frac{1}{8\pi G\gamma^2 \Delta} \{ \sin(\bar{\mu}'_2 c_2) \sin(\bar{\mu}'_3 c_3) + \text{cyclic terms} \}, \quad (3.21)$$

where ρ_ϕ is the matter density of ϕ :

$$\rho_\phi := \frac{p_\phi^2}{2p_1 p_2 p_3} := \frac{p_\phi^2}{2p^3}, \quad (3.22)$$

and we define $p^3 := p_1 p_2 p_3$ for convenience. Because $|\sin(\bar{\mu}'_I c_I)| \leq 1$, the vanishing of the Hamiltonian constraint $H''_{\bar{\mu}'} = 0$ immediately implies

$$\rho_\phi \leq \frac{3}{8\pi G\gamma^2 \Delta} = 3\rho_{\text{Pl}}. \quad (3.23)$$

The fact that ρ_ϕ is bounded above implies that the big-bang singularity is resolved and the big bounce is expected to occur when the matter density approaches

Planckian density. The inequality of (3.23) is saturated for the perfectly isotropic universe (i.e. $\kappa_1 = \kappa_2 = \kappa_3 = 1/3$) but we shall see that the maximal value of ρ_ϕ is in general lower than $3\rho_{\text{Pl}}$ with anisotropies introduced. (Also see Appendix C of [10].)

To know the detailed dynamics for each individual p_I , in addition to the Hamiltonian constraint, we study the Hamilton's equations:

$$\frac{dp_\phi}{dt''} = \{p_\phi, H''_{\mu'}\} = 0 \Rightarrow p_\phi \text{ is constant}, \quad (3.24)$$

$$\frac{d\phi}{dt''} = \{\phi, H''_{\mu'}\} = p_\phi(p_1 p_2 p_3)^{-1}, \quad (3.25)$$

$$\begin{aligned} \frac{dc_1}{dt''} &= \{c_1, H''_{\mu'}\} = 8\pi G\gamma \frac{\partial H''_{\mu'}}{\partial p_1} \\ &= -8\pi G\gamma \frac{\rho_\phi}{p_1} \end{aligned} \quad (3.26)$$

$$\begin{aligned} & - \frac{\bar{\mu}'_1 c_1 \cos(\bar{\mu}'_1 c_1) [\sin(\bar{\mu}'_2 c_2) + \sin(\bar{\mu}'_3 c_3)]}{2\gamma \Delta p_1} \\ & + \frac{\bar{\mu}'_2 c_2 \cos(\bar{\mu}'_2 c_2) [\sin(\bar{\mu}'_1 c_1) + \sin(\bar{\mu}'_3 c_3)]}{2\gamma \Delta p_1} \\ & + \frac{\bar{\mu}'_3 c_3 \cos(\bar{\mu}'_3 c_3) [\sin(\bar{\mu}'_1 c_1) + \sin(\bar{\mu}'_2 c_2)]}{2\gamma \Delta p_1}, \\ \frac{dp_1}{dt''} &= \{p_1, H''_{\mu'}\} = -8\pi G\gamma \frac{\partial H''_{\mu'}}{\partial c_1} \quad (3.27) \\ &= \frac{\bar{\mu}'_1 \cos(\bar{\mu}'_1 c_1) [\sin(\bar{\mu}'_2 c_2) + \sin(\bar{\mu}'_3 c_3)]}{\gamma \Delta}. \end{aligned}$$

Note that substituting (2.51) into (3.27) gives

$$\begin{aligned} & \frac{\sin(\bar{\mu}'_1 c_1)}{\bar{\mu}'_1} \quad (3.28) \\ &= \frac{\gamma \mathbf{L}_1}{2} \left\{ \frac{H_1 + H_3}{\cos(\bar{\mu}'_2 c_2)} + \frac{H_1 + H_2}{\cos(\bar{\mu}'_3 c_3)} - \frac{H_2 + H_3}{\cos(\bar{\mu}'_1 c_1)} \right\}, \end{aligned}$$

which is the modification of (2.53) with quantum corrections.

From (3.26) and (3.27), we have

$$2p_1 \frac{dc_1}{dt''} = -c_1 \frac{dp_1}{dt''} + c_2 \frac{dp_2}{dt''} + c_3 \frac{dp_3}{dt''} - 16\pi G\gamma \rho_\phi, \quad (3.29)$$

which yields

$$\frac{d}{dt''} (p_I c_I - p_J c_J) = 0, \quad (3.30)$$

and hence, in accordance with the constant parameters used for classical solutions in (2.59), we set

$$p_I c_I = 8\pi G\gamma \hbar [\mathcal{K}_I + f(t)] \quad (3.31)$$

with the time-varying function $f(t)$. In the classical regime, $p_I c_I$ become constant and so does $f(t)$. Taking (3.31) into the classical Hamiltonian constraint (2.58), we have

$$\mathcal{K}_\phi^2 = 2\left((\mathcal{K}_2 + f(t))(\mathcal{K}_3 + f(t)) + \text{cyclic terms}\right), \quad (3.32)$$

which gives the limiting values for $f(t)$ in the classical regime:

$$f(t) \rightarrow 0 \text{ or } -\frac{2}{3}\mathcal{K} \quad \text{as } \bar{\mu}'_I c_I \rightarrow 0. \quad (3.33)$$

That is, starting with $f = 0$ (or $f = -2\mathcal{K}/3$) in the classical regime, f decreases (or increases) towards the big bounces and finally across the bounces f ends up with the other constant $f = -2\mathcal{K}/3$ (or $f = 0$) on the other side of the classical regime. Equivalently, it can be said that the big bounces connect the classical solutions specified by $\kappa_1, \kappa_2, \kappa_3$ on one asymptotic side with its “conjugate” counterpart on the other asymptotic side specified by the “conjugate” parameters:

$$\kappa_1, \kappa_2, \kappa_3 \longleftrightarrow \kappa_1 - \frac{2}{3}, \kappa_2 - \frac{2}{3}, \kappa_3 - \frac{2}{3}. \quad (3.34)$$

[Note that the conjugate parameters also satisfy the constraints (2.25) and (2.27).]

Substituting (3.31) into (3.21), $H''_{\mu'} = 0$ then gives the complicated constraint:

$$\begin{aligned} \frac{\ell_\Delta^6 \mathcal{K}_\phi^2}{2p^3} &= \sin\left(\frac{\ell_\Delta^3 (\mathcal{K}_2 + f)}{p^{3/2}}\right) \sin\left(\frac{\ell_\Delta^3 (\mathcal{K}_3 + f)}{p^{3/2}}\right) \\ &+ \text{cyclic terms}, \end{aligned} \quad (3.35)$$

where we define

$$\ell_\Delta^3 := 8\pi G\gamma \hbar \Delta^{1/2} \sim \ell_{\text{Pl}}^3 \quad (3.36)$$

for convenience. In particular, considering the classical limit: $f \rightarrow 0$ or $f \rightarrow -2\mathcal{K}/3$ and $p^{3/2} := \sqrt{p_1 p_2 p_3} \gg \ell_\Delta^3$, we can show that (3.35) implies (2.26).

Substituting (3.31) into (3.27) and regarding ϕ as the emergent time via (3.25), we have

$$\begin{aligned} \frac{1}{p_1} \frac{dp_1}{d\phi} &= \frac{8\pi G\hbar p^{3/2}}{p_\phi \ell_\Delta^3} \cos\left(\frac{\ell_\Delta^3 (\mathcal{K}_1 + f)}{p^{3/2}}\right) \quad (3.37) \\ &\times \left[\sin\left(\frac{\ell_\Delta^3 (\mathcal{K}_2 + f)}{p^{3/2}}\right) + \sin\left(\frac{\ell_\Delta^3 (\mathcal{K}_3 + f)}{p^{3/2}}\right) \right]. \end{aligned}$$

Similar to the case of (3.15), p_1 gets bounced once “ $\cos(\dots)$ ” term in (3.37) flips sign. This happens when

$$\cos\left(\frac{\ell_\Delta^3 (\mathcal{K}_1 + f)}{p^{3/2}}\right) = 0 \Rightarrow \mathcal{K}_1 + f = \frac{\pi p^{3/2}}{2 \ell_\Delta^3}. \quad (3.38)$$

Assuming p_2 and p_3 also get bounced roughly around the same moment, at which (3.38) is satisfied, we have the approximation:

$$\begin{aligned} \sin\left(\frac{\ell_\Delta^3 (\mathcal{K}_2 + f)}{p^{3/2}}\right) &= \sin\left(\frac{\pi}{2} + \frac{\ell_\Delta^3 (\mathcal{K}_2 - \mathcal{K}_1)}{p^{3/2}}\right) \quad (3.39) \\ &= \cos\left(\frac{\ell_\Delta^3 (\mathcal{K}_2 - \mathcal{K}_1)}{p^{3/2}}\right) \approx 1 - \frac{\ell_\Delta^6 (\mathcal{K}_2 - \mathcal{K}_1)^2}{2p^3} + \dots \end{aligned}$$

and similar result for $\sin(\ell_\Delta^3(\mathcal{K}_3 + f)/p^{3/2})$. Substituting (3.38), (3.39) and (2.26) into (3.35), we can solve:

$$\begin{aligned} \frac{\ell_\Delta^3}{p^{3/2}} &\approx \sqrt{2}\mathcal{K}^{-1}|\kappa_1 - \kappa_2|^{-1}|\kappa_1 - \kappa_3|^{-1} \\ &\times \left((\kappa_1^2 + \kappa_2^2 + \kappa_3^2) + (\kappa_1 - \kappa_2)(\kappa_1 - \kappa_3) \right. \\ &\quad \left. - \left([(\kappa_1^2 + \kappa_2^2 + \kappa_3^2) + (\kappa_1 - \kappa_2)(\kappa_1 - \kappa_3)]^2 \right. \right. \\ &\quad \left. \left. - 3(\kappa_1 - \kappa_2)^2(\kappa_1 - \kappa_3)^2 \right)^{1/2} \right)^{1/2} \\ &=: \mathcal{K}^{-1}F(\kappa_1; \kappa_2, \kappa_3). \end{aligned} \quad (3.40)$$

The approximation is very accurate provided that

$$\begin{aligned} F(\kappa_1; \kappa_2, \kappa_3)|\kappa_2 - \kappa_1| &\ll \pi, \\ F(\kappa_1; \kappa_2, \kappa_3)|\kappa_3 - \kappa_1| &\ll \pi \end{aligned} \quad (3.41)$$

$$\Rightarrow \frac{\ell_\Delta^6(\mathcal{K}_2 - \mathcal{K}_1)^2}{p^3}, \frac{\ell_\Delta^6(\mathcal{K}_3 - \mathcal{K}_1)^2}{p^3} \ll \pi^2. \quad (3.42)$$

The criterion (3.41) is satisfied for the “near-isotropic” solutions (i.e. $\kappa_1, \kappa_2, \kappa_3$ are not so different, or more precisely, $(\kappa_1 - \kappa_2)^2, (\kappa_1 - \kappa_3)^2 \ll \kappa_1^2 + \kappa_2^2 + \kappa_3^2$). In practice, however, we only need the left hand side of (3.41) to be fairly smaller than the right hand side in order to have (3.39) an good approximation, since the Taylor series of $\cos x = 1 - x^2/2 + \dots$ converges very rapidly. Therefore, for most solutions (even Kasner-like), we can infer from (3.40) that that big bounces take place up to three times, once in each direction when the matter density ρ_ϕ approaches one of the three critical values $\rho_{I,\text{crit}}$ given by the Planckian density $\rho_{\text{Pl}} := (8\pi G\gamma^2\Delta)^{-1}$ times a numerical factor:

$$\rho_{1,\text{crit}} \approx \frac{1}{2}\kappa_\phi^2 F^2(\kappa_1; \kappa_2, \kappa_3) \rho_{\text{Pl}}. \quad (3.43)$$

For the solutions far from isotropic and thus (3.41) is badly violated, the above approximation is no longer good. Nevertheless, the big bounces still take place as most as three times at the moments when the “ $\cos(\dots)$ ” term flips sign in (3.37). The matter density ρ_ϕ is still the indication of the bounce occurrence, although the critical values could be quite different from (3.43).

The differential equations (3.25)–(3.27) can be solved numerically for given initial conditions. [See Footnote 7

for specifying the initial condition. Here, given $p_I(\phi_0)$, \mathcal{K}_I and \mathcal{K}_ϕ , $f(\phi_0)$ can be obtained via (3.35) and then $c_I(\phi_0)$ are fixed by (3.31).] The evolutions of $p_I(\phi)$, $a_I(\phi)$ and $\rho_\phi(\phi)$ are depicted in parts (a), (b) and (c) respectively in FIG. 3 for Kasner-unlike solution and in FIG. 4 for Kasner-like solution. Note that in FIG. 3, the epochs of big bounces indicated by the dotted lines in (a) are very close to the moments corresponding to $\rho_{I,\text{crit}}$ indicated in (c). In FIG. 4, the moments indicated in (a) and those in (c) are quite close to each other but slightly different due to the fact that (3.41) is now only fairly satisfied. Furthermore, p_1, p_2, p_3 bounce roughly around the same time, contrast to the $\bar{\mu}$ -scheme, in which the epochs of bounces in different directions can be arbitrarily separate. Also notice that each individual curve of $p_I(\phi)$ and $\alpha_I(\phi)$ in logarithmic scale becomes a straight line before and after the bounce, but the slope is changed, showing that the bounces conjoin two conjugate classical solutions. Finally, as in the $\bar{\mu}$ -scheme, the planar collapse in the Kasner-like case is *not* resolved.

Contrast to the $\bar{\mu}$ -scheme dynamics, in which the directional density ϱ_I is the indication of bounces, it is the ordinary matter density ρ_ϕ that signals the occurrence of bounces in $\bar{\mu}'$ -scheme. Unlike ϱ_I , the quantity of ρ_ϕ is independent of the choice of \mathcal{V} since

$$\rho_\phi = \frac{p_\phi^2}{2p_1p_2p_3} = \frac{\mathbf{V}^2\dot{\phi}^2}{\mathbf{V}^2} = \frac{\dot{\phi}^2}{2}. \quad (3.44)$$

Furthermore, (3.28) implies that the quantity $\bar{\mu}'c_I$ depends only on H_1, H_2, H_3 and is independent of \mathcal{V} . Consequently, (3.31) and (3.35) tell us: For given initial physical conditions $\dot{\phi}|_{t_0}$ and $H_I|_{t_0}$, \mathcal{K}_ϕ , \mathcal{K}_I and $f(t)$ all scale as $\propto \mathbf{V}|_{t_0}$. Therefore, the effective dynamics given by (3.37) is *completely independent* of the choice of \mathcal{V} as is the classical dynamics. In particular, the choice of \mathcal{V} has no effect on the numerical factor $\kappa_\phi^2 F^2(\kappa_I; \kappa_J, \kappa_K)/2$ appearing in (3.43). This is a desirable feature which $\bar{\mu}$ -scheme does not have. [However, if we further impose the quantum corrections on the eigenvalue of the inverse triad operator as mentioned in (3.3), this invariance is broken again.]

Even though $\bar{\mu}'$ -scheme is independent of \mathcal{V} , in case when \mathcal{V} has a global meaning, the bounce condition ($\rho_\phi \approx \rho_{I,\text{crit}}$) can be understood as: The *physical volume* of \mathcal{V} ($p^{3/2} = \mathbf{V}$) gets bounced when it undergoes the Planck regime (times a numerical value $2\kappa_\phi^{-2}F^{-2}(\kappa_I; \kappa_J, \kappa_K)$) measured by the reference of the momentum p_ϕ .

IV. SCALING SYMMETRY AND RELATIONAL MEASUREMENTS

With LQC discreteness corrections, both the $\bar{\mu}$ - and $\bar{\mu}'$ -schemes show that the big bang singularity (both Kasner-

like and Kasner-unlike) is resolved and replaced by the big bounces. The indication of the bounces is the directional densities ϱ_I in $\bar{\mu}$ -scheme whereas it is the matter density ρ_ϕ in $\bar{\mu}'$ -scheme. The detailed evolution of each individual p_I shows that the bounces occur up to three times, once in each direction, when ϱ_I in $\bar{\mu}$ -scheme or ρ_ϕ

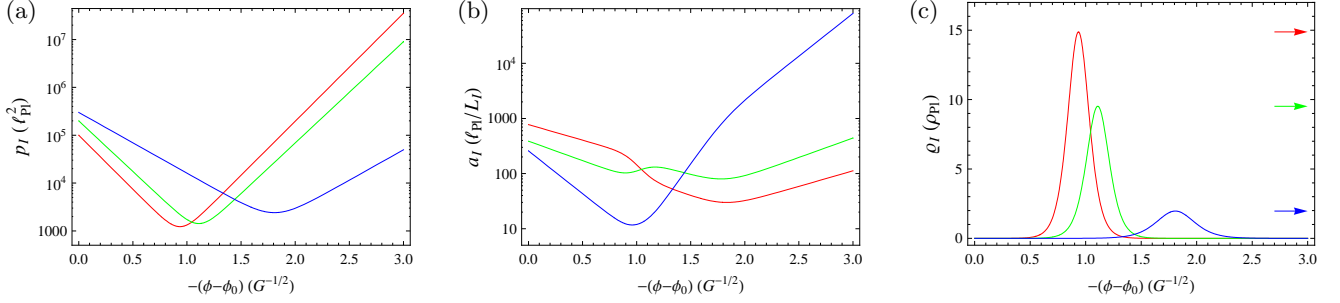


FIG. 1: **Kasner-unlike solution in $\bar{\mu}$ -scheme effective dynamics.** $\kappa_1 = 1/5$, $\kappa_2 = 1/4$, $\kappa_3 = 11/20$, $\kappa_\phi = \sqrt{119/200}$; $p_1(\phi_0) = 1. \times 10^5 \ell_{\text{Pl}}^2$, $p_2(\phi_0) = 2. \times 10^5 \ell_{\text{Pl}}^2$, $p_3(\phi_0) = 3. \times 10^5 \ell_{\text{Pl}}^2$; and $p_\phi = 2. \times 10^3 \hbar \sqrt{8\pi G}$ (i.e., $\mathcal{K}\kappa_\phi = 2. \times 10^3$). The red lines are for p_1 , a_1 , q_1 ; green for p_2 , a_2 , q_2 ; and blue for p_3 , a_3 , q_3 . The values of $q_{I, \text{crit}}$ given by (3.18) are pointed by the arrows in (c). (The Barbero-Immirzi parameter is set to $\gamma = 1$.)

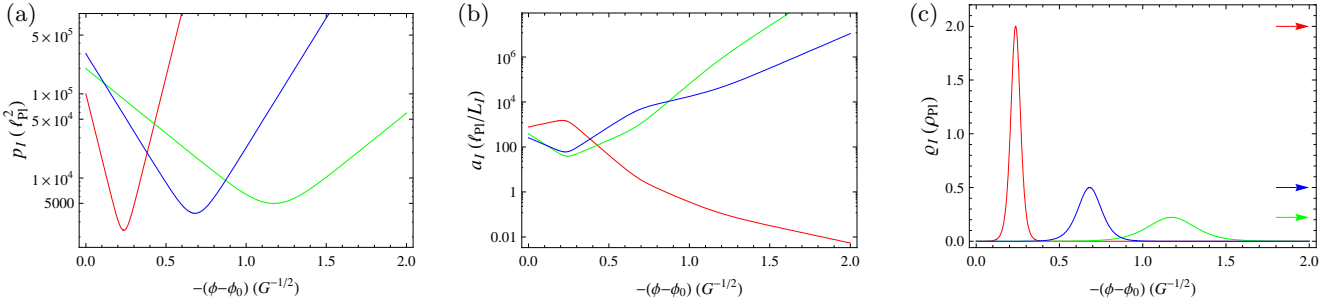


FIG. 2: **Kasner-like solution in $\bar{\mu}$ -scheme effective dynamics.** $\kappa_1 = -1/4$, $\kappa_2 = 3/4$, $\kappa_3 = 1/2$, $\kappa_\phi = 1/\sqrt{8}$; $p_1(\phi_0) = 1. \times 10^5 \ell_{\text{Pl}}^2$, $p_2(\phi_0) = 2. \times 10^5 \ell_{\text{Pl}}^2$, $p_3(\phi_0) = 3. \times 10^5 \ell_{\text{Pl}}^2$; and $p_\phi = 2. \times 10^3 \hbar \sqrt{8\pi G}$ (i.e., $\mathcal{K}\kappa_\phi = 2. \times 10^3$).

in $\bar{\mu}'$ -scheme approaches its critical value.

On the other hand, the planar collapse is *not* resolved but one of the length scale factors a_I continues the vanishing behavior in the Kasner-like case. This is expected since the classical solutions (2.59) and (2.62) yield $\bar{\mu}_I c_I, \bar{\mu}'_I c_I \rightarrow 0$ (and also $\mu_I^2 c_I \rightarrow 0$ in the μ_σ -scheme) toward the planar collapse and therefore the quantum corrections become more and more negligible.

The fact that smallness of p_I (not of a_I) signals the occurrence of big bounces seems to support the suggestion that “area is more fundamental than length in LQG”, although whether this is simply a technical artifact or reflects some deep physics is still not clear. (See Section VII.B of [16] for some comments on this aspect and [17] for more details.) Meanwhile, as the length operator has been shown to have a discrete spectrum [18], the fact that the vanishing of the length scale factor in the planar collapse is not stopped seems to contradict the discreteness of the length spectrum. Whether we miss some important ingredients when imposing the fundamental discreteness of LQG in the LQC construction or indeed area is more essential than length remains an open question for further investigation.

It has also been noted that the classical dynamics and the effective dynamics in $\bar{\mu}'$ -scheme are both independent of the choice of the finite sized cell \mathcal{V} , while the effective

dynamics in $\bar{\mu}$ -scheme depends on the physical size of \mathcal{V} . This can be rephrased in terms of the scaling symmetry;⁸ that is, the classical dynamics and $\bar{\mu}'$ -scheme effective dynamics are invariant under the following scaling:

$$\begin{aligned} p_1, p_2, p_3 &\longrightarrow l_2 l_3 p_1, l_1 l_3 p_2, l_1 l_2 p_3, \\ c_1, c_2, c_3 &\longrightarrow l_1 c_1, l_2 c_2, l_3 c_3, \\ p_\phi &\longrightarrow l_1 l_2 l_3 p_\phi, \\ \mathcal{K}_\phi &\longrightarrow l_1 l_2 l_3 \mathcal{K}_\phi, \\ \mathcal{K}_I &\longrightarrow l_1 l_2 l_3 \mathcal{K}_I. \end{aligned} \quad (4.1)$$

[Note that the scaling for \mathcal{K}_I should be accompanied by the same scaling on f in $\bar{\mu}'$ -scheme; in this case, that is $f \longrightarrow l_1 l_2 l_3 f$.] By contrast, the $\bar{\mu}$ -scheme does not respect this scaling except for the special case with $l_1 = l_2 = l_3$. In this sense, $\bar{\mu}$ -scheme has less symmetry of scaling than $\bar{\mu}'$ -scheme and the classical dynamics.

⁸ A dynamical system is said to be invariant under a certain scaling if for a given solution $(p_I(t), c_I(t), \phi(t))$ to the dynamics, the rescaled functions also satisfy the equations of motion (i.e. Hamilton’s equations and vanishing of Hamiltonian constraint). For classical dynamics, the equations to be satisfied are (2.15), (2.16) and (2.56)–(2.58); for $\bar{\mu}$ -scheme, (3.7)–(3.11); and for $\bar{\mu}'$ -scheme, (3.24)–(3.27) and (3.35).

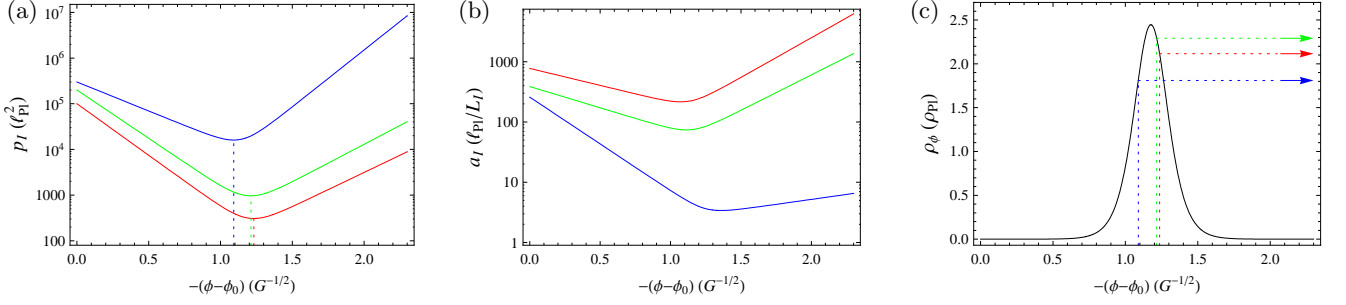


FIG. 3: **Kasner-unlike solution in $\bar{\mu}'$ -scheme effective dynamics.** $\kappa_1 = 1/5$, $\kappa_2 = 1/4$, $\kappa_3 = 11/20$, $\kappa_\phi = \sqrt{119/200}$; $p_1(\phi_0) = 1. \times 10^5 \ell_{\text{Pl}}^2$, $p_2(\phi_0) = 2. \times 10^5 \ell_{\text{Pl}}^2$, $p_3(\phi_0) = 3. \times 10^5 \ell_{\text{Pl}}^2$; and $p_\phi = 2. \times 10^3 \hbar \sqrt{8\pi G}$ (i.e., $\mathcal{K}\kappa_\phi = 2. \times 10^3$). The values of $\rho_{I,\text{crit}}$ given by (3.43) are pointed by the arrows in (c). The epochs of big bounces are indicated by dotted lines in (a), which are very close to the moments corresponding to $\rho_{I,\text{crit}}$, shown in (c).

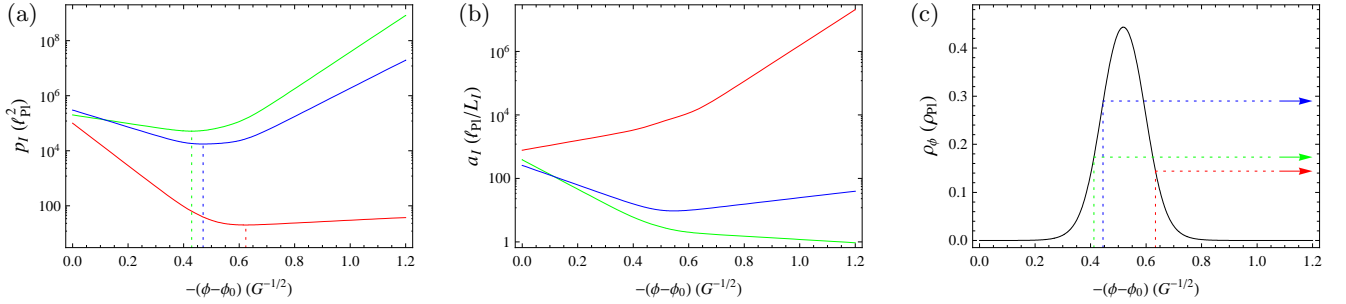


FIG. 4: **Kasner-like solution in $\bar{\mu}'$ -scheme effective dynamics.** $\kappa_1 = -1/4$, $\kappa_2 = 3/4$, $\kappa_3 = 1/2$, $\kappa_\phi = 1/\sqrt{8}$; $p_1(\phi_0) = 1. \times 10^4 \ell_{\text{Pl}}^2$, $p_2(\phi_0) = 2. \times 10^4 \ell_{\text{Pl}}^2$, $p_3(\phi_0) = 3. \times 10^4 \ell_{\text{Pl}}^2$; and $p_\phi = 2. \times 10^3 \hbar \sqrt{8\pi G}$ (i.e., $\mathcal{K}\kappa_\phi = 2. \times 10^3$). The epochs of big bounces are only slightly different from the moments corresponding to $\rho_{I,\text{crit}}$.

Apart from the scaling related to the dependence on \mathcal{V} , all three theories (classical, $\bar{\mu}$ -scheme, $\bar{\mu}'$ -scheme) also admit the scaling symmetry under:

$$\begin{aligned}
 \phi &\longrightarrow \lambda \phi, \\
 p_1, p_2, p_3 &\longrightarrow \lambda^{2/3} p_1, \lambda^{2/3} p_2, \lambda^{2/3} p_3, \\
 c_1, c_2, c_3 &\longrightarrow \lambda^{1/3} c_1, \lambda^{1/3} c_2, \lambda^{1/3} c_3, \\
 p_\phi &\longrightarrow \lambda p_\phi, \\
 \mathcal{K}_\phi &\longrightarrow \lambda \mathcal{K}_\phi, \\
 \mathcal{K}_I &\longrightarrow \lambda \mathcal{K}_I.
 \end{aligned} \tag{4.2}$$

This is reminiscent of the idea as suggested in [19, 20] that length/area/volume is measurable only if the line/surface/bulk is *coupled with the material reference*.

Another symmetry of scaling respected by the classical dynamics is given by

$$\begin{aligned}
 t &\longrightarrow \eta t, \\
 \gamma &\longrightarrow \xi \gamma, \\
 c_1, c_2, c_3 &\longrightarrow \xi \eta^{-1} c_1, \xi \eta^{-1} c_2, \xi \eta^{-1} c_3, \\
 p_\phi &\longrightarrow \eta^{-1} p_\phi, \\
 \mathcal{K}_\phi &\longrightarrow \eta^{-1} \mathcal{K}_\phi, \\
 \mathcal{K}_I &\longrightarrow \eta^{-1} \mathcal{K}_I.
 \end{aligned} \tag{4.3}$$

The scaling symmetry regarding $\gamma \longrightarrow \xi \gamma$ is expected, since the Barbero-Immirzi parameter γ has no effect on the classical dynamics. The scaling symmetry regarding $t \longrightarrow \eta t$ is also easy to understand, since there is no temporal scale introduced in the Hamiltonian. However, very surprisingly, the scaling symmetry involving $t \longrightarrow \eta t$ is violated for both $\bar{\mu}$ -scheme and $\bar{\mu}'$ -scheme effective dynamics. Curiously, this symmetry is restored if $t \longrightarrow \eta t$ is accompanied by $\gamma \longrightarrow \xi \gamma$ and one extra scaling is also imposed at the same time:

$$\Delta \longrightarrow \xi^{-2} \eta^2 \Delta. \tag{4.4}$$

This intriguing observation seems to suggest, albeit speculatively, that in the context of quantum gravity the fundamental scale (area gap) in spatial geometry gives rise to a temporal scale via the non-locality of quantum gravity (i.e., using holonomies) and the Barbero-Immirzi parameter γ somehow plays the role bridging the scalings in time and space. [This reminds us that, in LQG, the precise value of the area gap Δ is proportional to γ , and γ is also the parameter which relates the *intrinsic* geometry (encoded by spin connection Γ_a^i) with the *extrinsic* curvature (K_a^i) via $A_a^i = \Gamma_a^i - \gamma K_a^i$.]

Meanwhile, related to the above observations, the physical meaning of the directional factors ϱ_I and mat-

ter density ρ_ϕ can be interpreted as the (inverse of) area and volume scales, *measured by the reference of the matter content*. In this regard, we may say that the big bounces take place when one of the area scales or the volume scale becomes very small by the reference of the matter momentum. It is then tempting to regard not only ϕ as the “internal clock” (emergent time) but also p_ϕ as the “internal rod” — namely, the measurement of both temporal and spatial geometries makes sense only in the presence of matter content.

The observations about the symmetry of the scalings $\phi \rightarrow \lambda\phi$, $t \rightarrow \eta t$ and $\gamma \rightarrow \xi\gamma$ may support the ideas of the relational interpretation of quantum mechanics with real rods and clocks such as studied in [21] (see also [19, 20]), although the link is far from clear. However, as the theories studied in this paper are highly simplified, these observations could be just artifacts and we should not take this speculation too seriously until this aspect is further investigated for more sophisticated models.

V. SUMMARY AND OUTLOOK

To summarize, we list the important facts for the classical dynamics, $\bar{\mu}$ -scheme effective dynamics and $\bar{\mu}'$ -scheme effective dynamics in TABLE I. In the following, the main results are restated and some feasible extensions are remarked.

With the LQC discreteness corrections, the effective dynamics shows that the classical singularities (both Kasner-like and Kasner-unlike) are resolved and *replaced by the big bounces*, which take place *up to three times*, once in each diagonal direction. In $\bar{\mu}$ -scheme, it is the directional densities ϱ_I that signal the occurrence of big bounces whenever each of ϱ_I approaches its critical value. In $\bar{\mu}'$ -scheme, the indication is the matter density ρ_ϕ and the big bounces happen at the moments when ρ_ϕ approaches one of the three critical values.

Furthermore, the detailed evolution shows that the equations of motion (in terms of emergent time ϕ) for p_I in different diagonal directions are completely decoupled and evolve independently of one another in $\bar{\mu}$ -scheme; as a result the moments of three bounces can be arbitrarily separate. By contrast, in $\bar{\mu}'$ -scheme, equations of motion for p_I are coupled through ρ_ϕ and thus p_1 , p_2 , and p_3 bounce roughly around the same moment. In both schemes, there are three bounces in general unless the initial conditions are delicately fine tuned.

On the other hand, the planar collapse is *not* resolved but one of the length scale factors a_I continues the vanishing behavior in the Kasner-like case. Whether this suggests that area is more fundamental than length or conflicts with the discrete spectrum of length operator in LQG requires further investigation.

Across the bounces, the equations of motion again come closer and closer to the classical ones. Hence, the

Unfortunately, all the scaling symmetries break down in the detailed construction of LQC with $\bar{\mu}$ -scheme (the strategy to construct the full theory of LQC in $\bar{\mu}'$ -scheme is still not clear) even for the isotropic model (where $\bar{\mu}$ - and $\bar{\mu}'$ -schemes are identical). The full quantum theory only respects the scaling symmetries at the leading order. This is due to the fact that the quantum evolution in the full theory of LQC is governed by a difference equation, in which the step size of difference introduces an additional scale in the deep Planck regime (see [7] for Bianchi I model and [4] for the isotropic model). In fact, already in the level of effective dynamics, the scaling symmetries are violated if we further take into account the LQC corrections on the inverse triad as given by (3.3). For the full theory of LQC, if we take the aforementioned symmetries seriously, we might be able to revise the detailed construction in the spirit of relational quantum theory such that the step size in the difference equation scales adaptively by the reference of the matter content.

semiclassicality is retained on both asymptotic sides of the evolution. Given a classical solution in one asymptotic side, the evolution ends up with another classical solution on the other asymptotic side, which is either *antipodal* or *conjugate* to the given solution in $\bar{\mu}/\bar{\mu}'$ -scheme respectively.

In regard to the finite sized cell \mathcal{V} chosen to make sense of the Hamiltonian formalism, the effective dynamics in $\bar{\mu}$ -scheme depends on the choice of \mathcal{V} , and thereby reacts to the macroscopic scales introduced by the boundary conditions. (In terms of symmetry, it is said that $\bar{\mu}$ -scheme has less scaling symmetry than $\bar{\mu}'$ -scheme and classical dynamics.) The effective dynamics in $\bar{\mu}'$ -scheme, by contrast, is completely independent of \mathcal{V} as is the classical dynamics. (The issue of dependence on \mathcal{V} may be related to the instability of $\bar{\mu}$ -scheme indicated in [15].) In case that the physical size of \mathcal{V} has a global meaning (such as in the compactified Bianchi I model or the finite sized homogeneous patches in BKL scenario), the condition for the bounce occurrence can be rephrased: In $\bar{\mu}/\bar{\mu}'$ -scheme (respectively), the physical *area/volume* of the surfaces/bulk of \mathcal{V} gets bounced when it undergoes the Planck regime (times a numerical value) measured by the reference of the momentum p_ϕ .

While the $\bar{\mu}'$ -scheme has the advantage that its effective dynamics is independent of \mathcal{V} , the full theory of LQC based on $\bar{\mu}'$ -scheme is difficult to construct. Both $\bar{\mu}$ - and $\bar{\mu}'$ -schemes have desirable merits and it is still disputable which one is more faithful implementation of the underlying physics of quantum geometry.

In addition to the symmetry related to the choice of \mathcal{V} , both schemes admit additional symmetries of scaling, which are reminiscent of the relational interpretation of quantum mechanics, featuring the ideas of real rods and clocks. Furthermore, the symmetry involving the

classical dynamics	effective dynamics in $\bar{\mu}$ -scheme	effective dynamics in $\bar{\mu}'$ -scheme
$p_\phi = \hbar\sqrt{8\pi G}\mathcal{K}_\phi = \mathbf{V}\dot{\phi}$	$p_\phi = \hbar\sqrt{8\pi G}\mathcal{K}_\phi = \mathbf{V}\dot{\phi}$	$p_\phi = \hbar\sqrt{8\pi G}\mathcal{K}_\phi = \mathbf{V}\dot{\phi}$
$p_1 = L_2 L_3 (a_2 a_3) = \mathbf{L}_2 \mathbf{L}_3$	$p_1 = L_2 L_3 (a_2 a_3) = \mathbf{L}_2 \mathbf{L}_3$	$p_1 = L_2 L_3 (a_2 a_3) = \mathbf{L}_2 \mathbf{L}_3$
$c_I = \gamma \mathbf{L}_I H_I = \gamma \dot{\mathbf{L}}_I$	$\frac{\sin(\bar{\mu}_1 c_1)}{\bar{\mu}_1} = \frac{\gamma \mathbf{L}_1}{2} \left\{ \frac{H_1+H_3}{\cos(\bar{\mu}_2 c_2)} + \frac{H_1+H_2}{\cos(\bar{\mu}_3 c_3)} - \frac{H_2+H_3}{\cos(\bar{\mu}_1 c_1)} \right\}$	$\frac{\sin(\bar{\mu}'_1 c_1)}{\bar{\mu}'_1} = \frac{\gamma \mathbf{L}_1}{2} \left\{ \frac{H_1+H_3}{\cos(\bar{\mu}'_2 c_2)} + \frac{H_1+H_2}{\cos(\bar{\mu}'_3 c_3)} - \frac{H_2+H_3}{\cos(\bar{\mu}'_1 c_1)} \right\}$
$p_I c_I = 8\pi G \gamma \hbar \mathcal{K}_I = \gamma \mathbf{V} H_I$	$p_I \frac{\sin(\bar{\mu}_I c_I)}{\bar{\mu}_I} = 8\pi G \gamma \hbar \mathcal{K}_I$	$p_I c_I = 8\pi G \gamma \hbar [\mathcal{K}_I + f(t)]$ $f \rightarrow 0, -\frac{2}{3}\mathcal{K}$ in classical regime
$\mathcal{K}_\phi^2 = 2(\mathcal{K}_2 \mathcal{K}_3 + \mathcal{K}_1 \mathcal{K}_3 + \mathcal{K}_1 \mathcal{K}_2)$	$\mathcal{K}_\phi^2 = 2(\mathcal{K}_2 \mathcal{K}_3 + \mathcal{K}_1 \mathcal{K}_3 + \mathcal{K}_1 \mathcal{K}_2)$	$\mathcal{K}_\phi^2 = 2(\mathcal{K}_2 \mathcal{K}_3 + \mathcal{K}_1 \mathcal{K}_3 + \mathcal{K}_1 \mathcal{K}_2)$ and $\mathcal{K}_\phi^2 = 2 \left\{ \frac{p^3}{\ell_\Delta^3} \sin\left(\frac{\ell_\Delta^3(\mathcal{K}_2+f)}{p^{3/2}}\right) \sin\left(\frac{\ell_\Delta^3(\mathcal{K}_3+f)}{p^{3/2}}\right) + \text{cyclic terms} \right\}$
$\frac{1}{p_1} \frac{dp_1}{d\phi} = \frac{8\pi G \hbar}{p_\phi} (\mathcal{K}_2 + \mathcal{K}_3)$	$\frac{1}{p_1} \frac{dp_1}{d\phi} = \frac{8\pi G \hbar}{p_\phi} \cos(\bar{\mu}_1 c_1) (\mathcal{K}_2 + \mathcal{K}_3)$	$\frac{1}{p_1} \frac{dp_1}{d\phi} = \frac{8\pi G \hbar}{p_\phi} \cos\left(\frac{\ell_\Delta^3(\mathcal{K}_1+f)}{p^{3/2}}\right) \times \frac{p^{3/2}}{\ell_\Delta^3} \left\{ \sin\left(\frac{\ell_\Delta^3(\mathcal{K}_2+f)}{p^{3/2}}\right) + \sin\left(\frac{\ell_\Delta^3(\mathcal{K}_3+f)}{p^{3/2}}\right) \right\}$
$p_I \rightarrow 0$ toward singularity at the same moment	p_I bounces whenever $\varrho_I := \frac{p_\phi^2}{p_I^3} = \frac{\kappa_\phi^2}{\kappa_I^2} \rho_{PI}$; epochs of the bounces can be arbitrarily separate	p_1 bounces at the moment when $\rho_\phi := \frac{p_\phi^2}{2p_1 p_2 p_3} \approx \frac{1}{2} \kappa_\phi^2 F^2(\kappa_1; \kappa_2, \kappa_3) \rho_{PI}$; p_1, p_2, p_3 bounce roughly around the same moment
no big bounce; κ_I fixed	the big bounces conjoin the pair of “antipodal” classical solutions: $\kappa_I \longleftrightarrow -\kappa_I$	the big bounces conjoin the pair of “conjugate” classical solutions: $\kappa_I \longleftrightarrow \kappa_I - \frac{2}{3}$
symmetry of scaling: $t \longrightarrow \eta t$ $\gamma \longrightarrow \xi \gamma$ $\phi \longrightarrow \lambda \phi$ $p_1, p_2, p_3 \longrightarrow l_2 l_3 \lambda^{2/3} p_1, \dots$ $c_1, c_2, c_3 \longrightarrow l_1 \lambda^{1/3} \xi \eta^{-1} c_1, \dots$ $p_\phi \longrightarrow l_1 l_2 l_3 \lambda \eta^{-1} p_\phi$ $\mathcal{K}_\phi \longrightarrow l_1 l_2 l_3 \lambda \eta^{-1} \mathcal{K}_\phi$ $\mathcal{K}_I \longrightarrow l_1 l_2 l_3 \lambda \eta^{-1} \mathcal{K}_I$	symmetry of scaling: $t \longrightarrow \eta t$ $\gamma \longrightarrow \xi \gamma$ $\phi \longrightarrow \lambda \phi$ $p_1, p_2, p_3 \longrightarrow l^2 \lambda^{2/3} p_1, \dots$ $c_1, c_2, c_3 \longrightarrow l \lambda^{1/3} \xi \eta^{-1} c_1, \dots$ $p_\phi \longrightarrow l^3 \lambda \eta^{-1} p_\phi$ $\mathcal{K}_\phi \longrightarrow l^3 \lambda \eta^{-1} \mathcal{K}_\phi$ $\mathcal{K}_I \longrightarrow l^3 \lambda \eta^{-1} \mathcal{K}_I$ $\Delta \longrightarrow \xi^{-2} \eta^2 \Delta$	symmetry of scaling: $t \longrightarrow \eta t$ $\gamma \longrightarrow \xi \gamma$ $\phi \longrightarrow \lambda \phi$ $p_1, p_2, p_3 \longrightarrow l_2 l_3 \lambda^{2/3} p_1, \dots$ $c_1, c_2, c_3 \longrightarrow l_1 \lambda^{1/3} \xi \eta^{-1} c_1, \dots$ $p_\phi \longrightarrow l_1 l_2 l_3 \lambda \eta^{-1} p_\phi$ $\mathcal{K}_\phi \longrightarrow l_1 l_2 l_3 \lambda \eta^{-1} \mathcal{K}_\phi$ $(\mathcal{K}_I + f) \longrightarrow l_1 l_2 l_3 \lambda \eta^{-1} (\mathcal{K}_I + f)$ $\Delta \longrightarrow \xi^{-2} \eta^2 \Delta$

TABLE I: Summary of the classical dynamics, $\bar{\mu}$ -scheme effective dynamics and $\bar{\mu}'$ -scheme effective dynamics.

Barbero-Immirzi parameter is suggestive that the fundamental scale (area gap) in spatial geometry may give rise to a fundamental scale in temporal measurement. These symmetries however break down in the construction for the full theory of LQC.

A few possible extensions following the treatment of this paper seem to be within reach. First, as this paper focuses specifically on the model with a massless scalar field, it should be straightforward (with necessary approximation) to extend the results to the models with inclusion of generic matters, which will fulfill the investigation in [10] for the $\bar{\mu}'$ -scheme. Another extension involves the inclusion of nontrivial potentials for the scalar field. In both extensions, most of the observations we obtained here are to be expected and the investigations in broader context would further support or oppose some of our speculations.

Second, it would be instructive to compare the re-

sults of this paper with the perturbative treatment of anisotropies, since it has been suggested that the big bang singularity is not resolved if anisotropies are treated as perturbations of an isotropic background [22]. Incorporation of inhomogeneities, on the other hand, will be substantially more difficult. In order to determine whether $\bar{\mu}$ - or $\bar{\mu}'$ -scheme is more physically sensible, we have to incorporate inhomogeneities at least approximately or perturbatively in the background of Bianchi I type. The perturbative treatment such as developed in [23] or the strong gravity approximation proposed in [24] might be useful for this purpose.

Finally, the results in principle could be extended to the Bianchi IX model. Since Bianchi IX model, along with Bianchi I model, plays a pivotal role for the infinite fragmentation of the homogeneous patches close to the singularity in the BKL scenario, the analysis may provide hints to how the loop quantum effects resolve the classical

singularities in generic situations and in return it may help arbitrate the tension between $\bar{\mu}$ - and $\bar{\mu}'$ -schemes for the Bianchi I model.

Acknowledgments

The author is grateful for the valuable discussions with Abhay Ashtekar, Martin Bojowald, Golam Hossain, Kevin Vandersloot and especially Tomasz Pawłowski and Parampreet Singh, who helped clarify confusions and inspired important ideas. This work was supported in part by the NSF grant PHY-0456913.

APPENDIX A: EFFECTIVE DYNAMICS IN μ_o -SCHEME

One of the virtues of the improved strategy ($\bar{\mu}$ -scheme) in the isotropic model is to fix the serious drawback in the old precursor strategy (μ_o -scheme) that the critical value of the matter density at which the bounce occurs can be made arbitrarily small by increasing the momentum p_ϕ , thereby leading to wrong semiclassical behavior.

In the Bianchi I model, either the directional densities ϱ_I (in $\bar{\mu}$ -scheme) or the matter density ρ_ϕ (in $\bar{\mu}'$ -scheme) plays the same role as ρ_ϕ does in the isotropic case. Having learned from the isotropic case, we expect that the critical values of ϱ_I or ρ_ϕ at which the bounces occur can be made arbitrarily small by increasing the momentum p_ϕ in μ_o -scheme but is independent of p_ϕ in $\bar{\mu}$ - or $\bar{\mu}'$ -scheme. The latter is what has been shown in the main text of this paper.⁹ For comparison, the effective dynamics in μ_o -scheme is presented here.¹⁰

In the effective theory of μ_o -scheme, we take the prescription to replace c_I by $\sin(\mu_I^\circ c_I)/\mu_I^\circ$ with the *fixed* numbers μ_I° for discreteness. Analogous to (3.4), we have the effective (rescaled) Hamiltonian constraint:

$$H'_{\mu_o} = \frac{p_\phi^2}{2} - \frac{1}{8\pi G\gamma^2} \left\{ \frac{\sin(\mu_2^\circ c_2) \sin(\mu_3^\circ c_3)}{\mu_2^\circ \mu_3^\circ} p_2 p_3 + \text{cyclic terms} \right\}. \quad (\text{A1})$$

Again, the equations of motion are given by the Hamilton's equations and the constraint that the Hamiltonian must vanish:

$$\frac{dp_\phi}{dt'} = \{p_\phi, H'_{\mu_o}\} = 0 \Rightarrow p_\phi \text{ is constant}, \quad (\text{A2})$$

$$\frac{d\phi}{dt'} = \{\phi, H'_{\mu_o}\} = p_\phi, \quad (\text{A3})$$

⁹ The critical values $\varrho_{I,\text{crit}}$ depend on p_ϕ only through the ratios κ_ϕ^2/κ_I^2 in $\bar{\mu}$ -scheme; $\rho_{I,\text{crit}}$ depends on p_ϕ only through $\kappa_\phi^2 F^2(\kappa_I; \kappa_J, \kappa_K)/2$ in $\bar{\mu}'$ -scheme.

¹⁰ For the Bianchi I LQC, the effective dynamics in μ_o -scheme was first studied in [8] for the vacuum solution.

$$\begin{aligned} \frac{dc_1}{dt'} &= \{c_1, H'_{\mu_o}\} = 8\pi G\gamma \frac{\partial H'_{\mu_o}}{\partial p_1} \\ &= -\gamma^{-1} \frac{\sin(\mu_1^\circ c_1)}{\mu_1^\circ} \\ &\quad \times \left[\frac{\sin(\mu_2^\circ c_2)}{\mu_2^\circ} p_2 + \frac{\sin(\mu_3^\circ c_3)}{\mu_3^\circ} p_3 \right], \quad (\text{A4}) \end{aligned}$$

$$\begin{aligned} \frac{dp_1}{dt'} &= \{p_1, H'_{\mu_o}\} = -8\pi G\gamma \frac{\partial H'_{\mu_o}}{\partial c_1} \\ &= \gamma^{-1} p_1 \cos(\mu_1^\circ c_1) \\ &\quad \times \left[\frac{\sin(\mu_2^\circ c_2)}{\mu_2^\circ} p_2 + \frac{\sin(\mu_3^\circ c_3)}{\mu_3^\circ} p_3 \right], \quad (\text{A5}) \end{aligned}$$

as well as

$$H'_{\mu_o}(c_I, p_I) = 0 \Rightarrow p_\phi^2 = \frac{1}{4\pi G\gamma^2} \left\{ \frac{\sin(\mu_2^\circ c_2) \sin(\mu_3^\circ c_3)}{\mu_2^\circ \mu_3^\circ} p_2 p_3 + \text{cyclic terms} \right\}. \quad (\text{A6})$$

From (A4) and (A5), we have

$$\frac{d}{dt'} \left[p_I \frac{\sin(\mu_I^\circ c_I)}{\mu_I^\circ} \right] = 0, \quad (\text{A7})$$

which gives

$$p_I \frac{\sin(\mu_I^\circ c_I)}{\mu_I^\circ} = 8\pi G\gamma \hbar \mathcal{K}_I. \quad (\text{A8})$$

Taking (A8) into (A6) gives the same constraints on the constant parameters as in (2.26).

Substituting (A8) into (A5) yields

$$\frac{1}{p_1} \frac{dp_1}{dt'} = 8\pi G\hbar \cos(\mu_1^\circ c_1) (\mathcal{K}_2 + \mathcal{K}_3). \quad (\text{A9})$$

By (A3) and $\cos x = \pm \sqrt{1 - \sin^2 x}$, (A9) leads to

$$\frac{1}{p_I} \frac{dp_I}{d\phi} = \pm \sqrt{8\pi G} \left(\frac{1 - \kappa_I}{\kappa_\phi} \right) \left[1 - \left(\frac{\varrho_I}{\varrho_{I,\text{crit}}^{\mu_o}} \right)^{2/3} \right]^{1/2}, \quad (\text{A10})$$

which gives the bouncing solutions with the behaviors similar to those given by (3.16) except that the critical value of ϱ_I at which the big bounce takes place is given by

$$\varrho_{I,\text{crit}}^{\mu_o} := \left[\left(\frac{\kappa_\phi}{\kappa_I} \right)^2 \frac{\rho_{\text{Pl}} \Delta}{\mu_I^{\circ 2}} \right]^{3/2} \frac{1}{p_\phi}, \quad (\text{A11})$$

which can be made arbitrarily small by increasing the value of p_ϕ . As a result, μ_o -scheme gives wrong semiclassical behavior and should be improved by $\bar{\mu}$ - or $\bar{\mu}'$ -scheme to fix this problem.

APPENDIX B: QUANTIZATION IN THE $\bar{\mu}$ -SCHEMES

In this appendix, we give a heuristic argument for the prescription given by (3.1), starting from the Hamiltonian constraint of LQG. The motivations for both $\bar{\mu}$ - and $\bar{\mu}'$ -schemes are addressed in detail. The advantages and drawbacks of both schemes are also remarked.

The gravitational part of the classical Hamiltonian constraint in the full theory of LQG is given by

$$\begin{aligned} H_{\text{grav}} &= \frac{1}{8\pi G} \int d^3x N e^{-1} \left\{ \epsilon_i{}^{jk} F_{ab}^i \tilde{E}^a{}_j \tilde{E}^b{}_k \right. \\ &\quad \left. - 2(1 + \gamma^2) K_{[a}{}^i K_{b]}^j \tilde{E}^a{}_i \tilde{E}^b{}_j \right\} \\ &= -\frac{1}{8\pi G \gamma^2} \int d^3x N e^{-1} \epsilon_i{}^{jk} F_{ab}^i \tilde{E}^a{}_j \tilde{E}^b{}_k, \quad (\text{B1}) \end{aligned}$$

where $e := |\det \tilde{E}|^{1/2}$ and in the last line we exploit the fact that for homogeneous and spatially flat models the two terms inside the curly bracket are proportional to each other (because $-\gamma K_a{}^i = A_a{}^i$ as the spatial slice is flat and $F_{ab}^i = \epsilon^i{}_{jk} A_a{}^j A_b{}^k$ as it is homogeneous). Furthermore, the lapse N can be assumed to be constant because of homogeneity and we set $N = 1$.

When applied to Bianchi I models, the integral is restricted to a finite sized cell \mathcal{V} as prescribed by (2.6). Accordingly, we should also adopt the replacement rules (2.39) and (2.40). This procedure gives

$$\begin{aligned} H_{\text{grav}} &= -\frac{1}{8\pi G \gamma^2} \int_{\mathcal{V}} d^3x e^{-1} V_o^{-2} V^{-2} \\ &\quad \times \left(\epsilon_i{}^{jk} \epsilon^l{}_{lm} A_p{}^l A_q{}^m E^p{}_j E^q{}_k \right) \\ &= -\frac{1}{8\pi G \gamma^2} \int_{\mathcal{V}} d^3x e^{-1} V_o^{-2} V^{-2} \\ &\quad \times (\tilde{c}_2 \tilde{c}_3 \tilde{p}_2 \tilde{p}_3 + \text{cyclic terms}) \\ &= -\frac{(c_2 c_3 p_2 p_3 + \text{cyclic terms})}{8\pi G \gamma^2 e V} \quad (\text{B2}) \end{aligned}$$

and

$$\begin{aligned} e^2 &= |\det \tilde{E}| = V^{-3} |\det(E^j{}_i e_j^a)| \\ &= V^{-3} \left| \frac{\tilde{p}_1 \tilde{p}_2 \tilde{p}_3}{a_1 a_2 a_3} \right| = V^{-2} |p_1 p_2 p_3|. \quad (\text{B3}) \end{aligned}$$

Consequently, we have

$$H_{\text{grav}} = -\frac{(c_2 p_2 c_3 p_3 + c_1 p_1 c_3 p_3 + c_1 p_1 c_2 p_2)}{8\pi G \gamma^2 \sqrt{|p_1 p_2 p_3|}}, \quad (\text{B4})$$

which is exactly the same as H_{grav} given in (2.54).

When the quantization is performed in the context of LQC, there are two loop quantum corrections. The first is the modification on the inverse triad operator $1/\sqrt{|p_I|}$ as indicated in (3.3), which is negligible and ignored in this paper. The second is due to the fact that the connections

$A_a{}^i$ (or c_I) do not exist and should be replaced with holonomies (or exponentials of c_I).

Following the standard techniques in gauge theories, the curvature component F_{ab}^i can be expressed in terms of holonomies (i.e. Wilson loops). Given a small surface α center in \vec{x} , Stokes' theorem allows us to write the curvature component as

$$\begin{aligned} \tau_i F_{ab}^i(\vec{x}) &\approx \frac{1}{\epsilon_{ab}^\alpha} \int_\alpha \tau_i F_{cd}^i dx^c \wedge dx^d \\ &\approx \frac{1}{\epsilon_{ab}^\alpha} \left[\mathcal{P} \exp \left(\oint_{\partial\alpha} \tau_i A_c{}^i dx^c \right) - 1 \right], \quad (\text{B5}) \end{aligned}$$

where $2i\tau_i = \sigma_i$ are the Pauli matrices; $\partial\alpha$ is the boundary loop of α ; and the *coordinate* area of α projected in “ ab -direction” is given by

$$\epsilon_{ab}^\alpha = \int_\alpha dx^a \wedge dx^b. \quad (\text{B6})$$

This is a good approximation provided ϵ_{ab}^α is small enough and in fact it becomes exact in the continuous limit $\epsilon_{ab}^\alpha \rightarrow 0$.

For the Bianchi I model, we choose $\alpha = \square_{JK}$ to be a small rectangular surface parallel to the J - K plane. The *coordinate* lengths of the edges of α are denoted as $\bar{\mu}_J L_K$ and $\bar{\mu}_K L_J$ and accordingly the *coordinate* area is given by $\epsilon_{JK}^\alpha \equiv \epsilon_{JK}^\square = \bar{\mu}_J \bar{\mu}_K L_J L_K$ (see FIG. 5). Applying (2.40) and noting that $F_{ab}^i = \epsilon^i{}_{jk} A_a{}^j A_b{}^k$ gives

$$F_{ab}^i \longrightarrow F_{JK}^I := \epsilon_{IJK} (L_J L_K)^{-1} c_J c_K, \quad (\text{B7})$$

we read off from (B5) that

$$F_{JK}^I \approx -\frac{2}{\epsilon_{JK}^\square} \text{Tr} \left[\tau_I \left(h_{JK}^{(\bar{\mu}_J, \bar{\mu}_K)} - 1 \right) \right], \quad (\text{B8})$$

where (I, J, K) is any permutation of $(1, 2, 3)$ and the holonomy along the edges of \square_{JK} is:

$$h_{\square_{JK}}^{(\bar{\mu}_J, \bar{\mu}_K)} := h_J^{(\bar{\mu}_J)} h_K^{(\bar{\mu}_K)} (h_J^{(\bar{\mu}_J)})^{-1} (h_K^{(\bar{\mu}_K)})^{-1} \quad (\text{B9})$$

with $h_I^{(\bar{\mu}_I)}$ being the holonomy along the individual edge:

$$\begin{aligned} h_I^{(\bar{\mu}_I)} &:= \mathcal{P} \exp \left(\int_0^{\bar{\mu}_I L_I} \tau_i A_a{}^i dx^a \right) \longrightarrow \exp(\bar{\mu}_I c_I \tau_I) \\ &= \cos\left(\frac{\bar{\mu}_I c_I}{2}\right) + 2 \sin\left(\frac{\bar{\mu}_I c_I}{2}\right) \tau_I, \quad (\text{B10}) \end{aligned}$$

which follows

$$\text{Tr} \left[\tau_I h_{\square_{JK}}^{(\bar{\mu}_J, \bar{\mu}_K)} \right] = -\frac{\epsilon_{IJK}}{2} \sin(\bar{\mu}_J c_J) \sin(\bar{\mu}_K c_K). \quad (\text{B11})$$

Putting (B7), (B8) and (B11) altogether, we then have

$$c_J c_K \approx \frac{\sin(\bar{\mu}_J c_J) \sin(\bar{\mu}_K c_K)}{\bar{\mu}_J \bar{\mu}_K}, \quad (\text{B12})$$

which is exactly the prescription used in (3.1).

If \square_{JK} shrinks to a point, this gives the continuous limit $\bar{\mu}_I \rightarrow 0$ and we recover the classical Hamiltonian constraint in (B4). However, the very feature of LQC is that the continuous limit does not exist and the failure of the limit to exist is intimately related with the underlying quantum geometry of LQG, where eigenvalues of the area operator are *discrete*. In LQC, to implement the discreteness as imprint from the full theory of LQG, we have to set $\bar{\mu}_I$ to be finite. The question now is: What values should $\bar{\mu}_I$ be set to faithfully reflect the fundamental discreteness of quantum geometry? Two strategies ($\bar{\mu}$ - and $\bar{\mu}'$ -schemes) are discussed below.

Since the eigenvalue spectrum of the area operator has an *area gap* Δ , to impose the discreteness, it is straightforward to set the *physical* area of \square_{JK} to be Δ (depicted in FIG. 5.a); i.e.

$$\begin{aligned} a_J a_K \epsilon_{JK}^{\square} &= a_J a_K \bar{\mu}_J \bar{\mu}_K L_J L_K \\ &= |\epsilon_{IJK} p_I| \bar{\mu}_J \bar{\mu}_K = \Delta, \end{aligned} \quad (\text{B13})$$

which gives the “ $\bar{\mu}'$ -scheme” in (3.6).

However, a closer consideration seems to suggest that equating the physical area of \square_{JK} to Δ might not be completely sensible. Recall that the validity of (B5) is based on Stokes’ theorem, which does *not* invoke the metric of the surface α at all. The smallness of α to ensure good approximation of (B5) does not directly refer to metric smallness, either. Furthermore, if we think of the picture of spin networks in LQG, what associated with the physical areas are links (holonomies) of the spin network; the area enclosed by the loop of holonomy links is irrelevant! Therefore, back to LQC, instead of shrinking the area of \square_{JK} , we should associate each *edge* of \square_{JK} with an area and then shrink the associated areas to Δ . (See FIG. 5.b.) The edge of \square_{JK} in J -direction is of *coordinate* length $\bar{\mu}_J L_J$, with which, most naturally, we associate a rectangle \square_J parallel to I - K plane of *coordinate* lengths $\bar{\mu}_J L_I$ and $\bar{\mu}_J L_K$ on its edges. (That is, the ratio of the edge of \square_J to the edge of \mathcal{V} in the I/K -direction is set to be the same as the ratio of the edge of \square_{JK} to the edge of \mathcal{V} in the J -direction.) We then set the *physical* area of \square_J to Δ ; i.e.

$$a_I a_K \bar{\mu}_J^2 L_I L_K = \bar{\mu}_J^2 |p_J| = \Delta, \quad (\text{B14})$$

which gives the “ $\bar{\mu}$ -scheme” in (3.5).

[Note that in both pictures of $\bar{\mu}'$ - and $\bar{\mu}$ -schemes, if we rather set the *coordinate* area of \square_{JK} or \square_J to be Δ , we end up with constant $\bar{\mu}_I$. This is the “ μ_o -scheme” used in the precursor strategy. The wrong semiclassical behavior of the μ_o -scheme originates from the problem that the *coordinate* area (both of \square_{JK} and of \square_J) is not totally physically relevant.]

In the full theory of LQG, when the Hamiltonian acts on an spin network state, it adds a new link of spin-1/2 and the coloring of the links on which the new link is attached is increased or decreased by 1/2 (see FIG. 6.a-b). The resulting spin network state is equivalent to the original state superimposed with a triangular loop of spin-1/2

links (FIG. 6.c). This triangular loop is essentially the Wilson loop discussed above. From this perspective, the $\bar{\mu}'$ -scheme can be understood as associating the area in pink in FIG. 6.d with Δ , whereas the $\bar{\mu}$ -scheme as associating the area in blue in FIG. 6.e with Δ . In the context of spin network states, the coloring of a link corresponds to the area of the surface to which the link penetrates and the smallest coloring spin-1/2 gives rise to the *area gap* Δ . Therefore, it is in this sense that $\bar{\mu}$ -scheme is a more direct implementation of the underlying discreteness of quantum geometry than $\bar{\mu}'$ -scheme.

Furthermore, in the full quantum theory of LQC, $\bar{\mu}$ -scheme has the important virtue that we can define the affine variables v_I via

$$\frac{\partial}{\partial v_I} := 4\pi\gamma\ell_{\text{Pl}}^2 \bar{\mu}_I \frac{\partial}{\partial p_I} \quad (\text{B15})$$

such that Hamiltonian constraint of the full quantum theory gives the evolution as a difference equation in terms of v_I and therefore the methodology used for the isotropic LQC can be easily applied [7]. This strategy fails in $\bar{\mu}'$ -scheme since

$$\left[\bar{\mu}'_I \frac{\partial}{\partial p_I}, \bar{\mu}'_J \frac{\partial}{\partial p_J} \right] \neq 0 \quad (\text{B16})$$

and hence the corresponding affine variables do not exist. This makes it difficult to construct the full quantum theory of Bianchi I LQC in $\bar{\mu}'$ -scheme.

On the other hand, as studied in Section III, $\bar{\mu}'$ -scheme has the advantage over $\bar{\mu}$ -scheme that the effective dynamics in $\bar{\mu}'$ -scheme is independent of the choice of \mathcal{V} . The difference for this point between $\bar{\mu}$ - and $\bar{\mu}'$ -schemes can be understood, heuristically but instructively, by estimating the quantity $\bar{\mu}_I c_I$ with the classical formulae; that is, plugging (2.53) for c_I , we have

$$\bar{\mu}_I c_I \approx \gamma \Delta^{1/2} H_I \left(\frac{\mathbf{L}_1^2}{\mathbf{L}_2 \mathbf{L}_3} \right)^{1/2}, \quad (\text{B17})$$

$$\bar{\mu}'_I c_I \approx \gamma \Delta^{1/2} H_I. \quad (\text{B18})$$

Since the quantity $\bar{\mu}_I c_I$ indicates how significant the quantum corrections are (quantum corrections are negligible if $\bar{\mu}_I c_I \ll 1$), (B17) tells that in $\bar{\mu}$ -scheme, the place at which the quantum effects become appreciable is tied up with not only the Hubble rates H_I but also the physical geometry of \mathcal{V} . By contrast, (B18) shows that the different choice of \mathcal{V} is irrelevant in $\bar{\mu}'$ -scheme.

In the language of [15], $\bar{\mu}$ -scheme corresponds to a lattice refinement model whereby the number of vertices is proportional to the transverse area. A stability analysis suggests that $\bar{\mu}$ -scheme leads to an unstable difference equation in the full theory of LQC and thus may not represent a good quantization scheme.

Both $\bar{\mu}$ - and $\bar{\mu}'$ -schemes have desirable and undesirable features of their own. In order to understand them more deeply, in the main text we study both schemes and their ramifications at the level of effective dynamics.

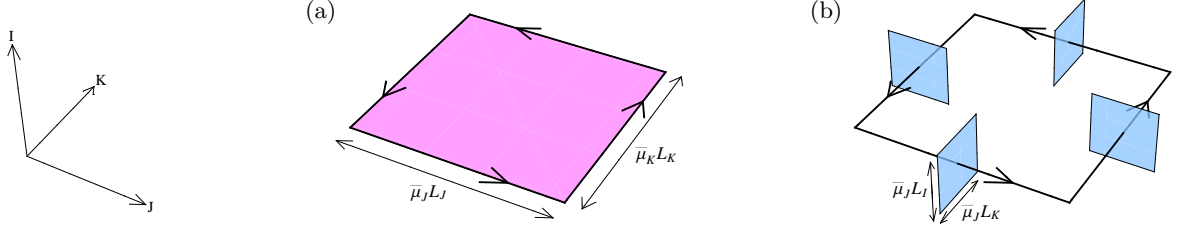


FIG. 5: **(a)** The surface in pink is \square_{JK} , the *physical* area of which is to be shrunk to Δ in the $\bar{\mu}'$ -scheme. **(b)** The surfaces in blue are \square_J and \square_K , the *physical* areas of which are to be shrunk to Δ in the $\bar{\mu}$ -scheme.

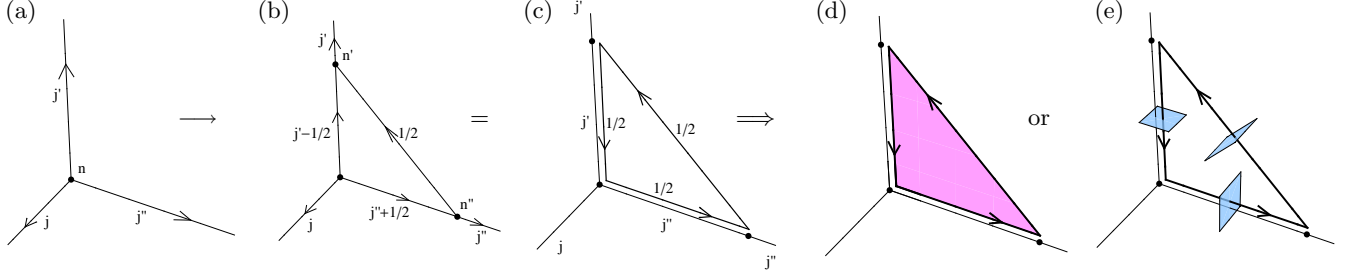


FIG. 6: **(a)-(b)** The action of Hamiltonian acting on a spin network state. **(c)** The resulting state is equivalent to the original one superposed with a triangular loop. **(d)** The idea of $\bar{\mu}'$ -scheme. **(e)** The idea of $\bar{\mu}$ -scheme.

-
- [1] M. Bojowald, “Loop quantum cosmology,” Living Rev. Rel. **8**, 11 (2005) [arXiv:gr-qc/0601085].
 - [2] A. Ashtekar, T. Pawłowski and P. Singh, “Quantum nature of the big bang: An analytical and numerical investigation I,” Phys. Rev. D **73**, 124038 (2006) [arXiv:gr-qc/0604013].
 - [3] A. Ashtekar, T. Pawłowski and P. Singh, “Quantum nature of the big bang,” Phys. Rev. Lett. **96**, 141301 (2006) [arXiv:gr-qc/0602086].
 - [4] A. Ashtekar, T. Pawłowski and P. Singh, “Quantum nature of the big bang: Improved dynamics,” Phys. Rev. D **74**, 084003 (2006) [arXiv:gr-qc/0607039].
 - [5] A. Ashtekar, T. Pawłowski, P. Singh and K. Vandersloot, “Loop quantum cosmology of $k = 1$ FRW models,” Phys. Rev. D **75**, 024035 (2007) [arXiv:gr-qc/0612104].
 - [6] K. Vandersloot, “Loop quantum cosmology and the $k = -1$ RW model,” Phys. Rev. D **75**, 023523 (2007) [arXiv:gr-qc/0612070].
 - [7] D. W. Chiou, “Loop quantum cosmology in Bianchi type I models: Analytical investigation,” Phys. Rev. D **75**, 024029 (2007) [arXiv:gr-qc/0609029].
 - [8] G. Date, “Absence of the Kasner singularity in the effective dynamics from loop quantum cosmology,” Phys. Rev. D **71**, 127502 (2005) [arXiv:gr-qc/0505002].
 - [9] D. W. Chiou, “Effective dynamics for the cosmological bounces in Bianchi type I loop quantum cosmology,” arXiv:gr-qc/0703010.
 - [10] D. W. Chiou and K. Vandersloot, “The behavior of non-linear anisotropies in bouncing Bianchi I models of loop quantum cosmology,” Phys. Rev. D **76**, 084015 (2007) [arXiv:0707.2548 [gr-qc]].
 - [11] D. C. Salisbury, J. Helpert and A. Schmitz, “Reparameterization invariants for anisotropic Bianchi I cosmology with a massless scalar source,” arXiv:gr-qc/0503014.
 - [12] P. Singh and K. Vandersloot, “Semi-classical states, effective dynamics and classical emergence in loop quantum cosmology,” Phys. Rev. D **72**, 084004 (2005) [arXiv:gr-qc/0507029].
 - [13] M. Bojowald, “Large scale effective theory for cosmological bounces,” Phys. Rev. D **75**, 081301 (2007) [arXiv:gr-qc/0608100].
 - [14] “Effective theory for Bianchi I models of loop quantum cosmology”, work in progress.
 - [15] M. Bojowald, D. Cartin and G. Khanna, “Lattice refining loop quantum cosmology, anisotropic models and stability,” Phys. Rev. D **76**, 064018 (2007) [arXiv:0704.1137 [gr-qc]].
 - [16] C. Rovelli, “Loop quantum gravity,” Living Rev. Rel. **1**, 1 (1998) [arXiv:gr-qc/9710008].
 - [17] C. Rovelli, “Area is the length of Ashtekar’s triad field,” Phys. Rev. D **47**, 1703 (1993).
 - [18] T. Thiemann, “A length operator for canonical quantum gravity,” J. Math. Phys. **39**, 3372 (1998) [arXiv:gr-qc/9606092].
 - [19] C. Rovelli, “What is observable in classical and quantum gravity?,” Class. Quant. Grav. **8**, 297 (1991).
 - [20] C. Rovelli, “A Generally covariant quantum field theory and a prediction on quantum measurements of geometry,” Nucl. Phys. B **405**, 797 (1993).
 - [21] R. Gambini and J. Pullin, “Relational physics with real rods and clocks and the measurement problem of quantum mechanics,” arXiv:quant-ph/0608243.

- [22] M. Bojowald, H. H. Hernandez and H. A. Morales-Tecotl, “Perturbative degrees of freedom in loop quantum gravity: Anisotropies,” *Class. Quant. Grav.* **23**, 3491 (2006) [arXiv:gr-qc/0511058].
- [23] M. Bojowald, “Loop quantum cosmology and inhomogeneities,” *Gen. Rel. Grav.* **38**, 1771 (2006) [arXiv:gr-qc/0609034].
- [24] A. Henderson, D. Sloan, “Connection between the strong coupling limit of gravity and the BKL conjecture,” to appear.